



Universitat de Lleida

Study and implementation of self-adaptive structures

Màster en Enginyeria Industrial

Yina Betancourt
7-9-2017

Index

1. Introduction	3
2. Methodology	3
3. Literature review	4
3.1. Heat transfer enhancement	4
3.2. Self-adaptive fins.....	7
3.2.1. Bimetallic beams clamped-clamped.....	8
3.2.2. Bimetallic cantilevers.....	8
3.2.3. Shape Memory Alloys (SMA)	9
4. Analytical study.....	10
4.1. Bimetallic beam clamped-clamped (Microvalve)	11
4.1.1. Model	11
4.1.2. Analytical study.....	12
4.1.3. Analytical results.....	14
4.2. Beam cantilever.....	17
4.2.1. Model	17
4.2.2. Analytical study.....	18
4.2.3. Analytical results.....	20
5. Numerical study of micro actuators	24
5.1. Study of the mesh sensibility	24
5.2. Buckling effect: Microvalve.....	24
5.3. Deflection effect: Bimetallic cantilever fin	27
5.4. Combination between deflection and buckling effect.....	30
5.5. Triangular fins	34
5.5.1. Model 1	34
5.5.2. Model 2	42
6. Conclusion.....	45
Bibliography.....	46
Appendix	47
1. Microvalve	47
1.1. Maximum deformation.....	47
1.2. Non-dimensional curves.....	48
2. Bimetallic strip	50
2.1. Impact of width	50

2.2.	Impact of thickness.....	51
2.3.	Profile of a bimetallic strip submitted to an increase of temperature for difference heat transfer coefficient.....	52

1. Introduction

In the last decades, micro-electromechanical systems (MEMS) have been developed due to the research advances in the semiconductors field. MEMS are miniaturized mechanical and electromechanical elements, which are fabricated using micro fabrication. Their main functionality is to control physical, optical or chemical quantities. To allow the communication between MEMS transducers and the outside world, integrated circuits (ICs) are used. The usage of ICs is focused in the signal treatment coming from MEMS, such as analogue-to-digital conversion, amplification, filtering or information processing. Therefore, MEMS and ICs are integrated and packaged together. Two methods can be used [1]:

- The multi-chip solution where MEMS and IC components are manufactured on separate substrates and after, they are hybridized in a final device. They can be called as multi-chip modules, but also when the device is created through vertical stacking of several IC chips are called 2.5D or 3D structures.
- The system-on-chip (SoC) solution where MEMS and IC components are manufactured on the same substrate.

That trend of integrating and packaging explained before contributes to higher power density, higher operating temperatures and reduced reliability. Moreover, local hot spots (which have much higher temperatures compared to the average die temperature) are common in these configurations. High temperatures contribute to a lower trusty performance of semiconductor materials that can cause a failure in the device. For these reason, cooling solutions able to remove as much as possible heat are a current issue, extremely important.

A new and variable structure to change spatially and temporally the capacity of local heat removal through self-adaptive longitudinal vortex generators (LVGs) are studied in this project. The main objective to achieve with these structures is the raising up of the LVGs, also called fins, when the heat flux on the substrate is elevated and the return back of the fins to a plain position when the temperature of the substrate is low. Therefore, the ideal solution is that LVGs move in function of substrate temperature. It is very important the highest tip deflection of the fin to create more turbulence within the micro channel (MC), thus increasing the heat transfer between the coolant and the hot zone.

2. Methodology

The steps followed to achieve this project started with the literature review. First, micro cooling systems were reviewed to know the recent advances and see what could be the innovative and improved solutions for micro cooling applications.

Then, a bibliographic research of different self-adaptive materials has been done. Basically, bimetallic materials and shape memory alloy (SMA) were reviewed at the micro scale and for cooling applications because the main objective to achieve is the movement of the fins in function of the temperature. The phenomenons studied were based in the thermal expansion and constraints of the materials in some geometries. Thus, the structures reviewed are micro valves, bimetallic strips and SMAs.

On the other hand, mathematical models were implemented via Matlab. Matlab is a multi-paradigm numerical computing language developed by MathWorks, which allows matrix manipulations, plotting of functions and data, implementation of algorithms, creation of user interfaces, etc. The objective of this mathematical study was the optimisation of the main dimensions of self-adaptive structures to reach the highest deflection; this structures are a microvalve and a bimetallic cantilever. In this case, some mathematical equations are required to define the performance of the structures when they are submitted to an increase of temperature. The mathematical scripts in Matlab are showed in the appendix of this project.

In addition, some complex structures that take advantage of material's thermal expansion and constraints in the geometry are designed via COMSOL Multiphysics. COMSOL is a finite element analysis, solver and simulation software package for various physics and engineering applications, especially coupled phenomena, or Multiphysics. The interface of COMSOL is very different from Matlab. In this software it is required the modelling of the geometry, the definition of the materials and the introduction of the physics modules which are involved in the simulation. In this case, the modules were the heat transfer and the structural modules. It is not required to know the equation of each geometry or structure, because COMSOL uses them by default. This is why it is useful when a fin's design is very complex. Moreover, parametric studies can be made, since the dimension can be changed and combined in the desired range, to find the optimal fin geometry in order to reach the highest deflection.

Results are presented for each fin's model showing the geometry, the boundary conditions and optimal dimensions that makes the tip deflection the highest.

Finally, all the designs studied are compared in order to know which one is the best option to achieve the main objective of this project.

3. Literature review

In this section is made a literature review of the advances in the heat transfer enhancement in micro channels. Additionally, self-adaptive fins of different materials are reviewed.

3.1. Heat transfer enhancement

First cooling technologies used heat pipes, vapour chambers, high performance interface materials and high performance air moving devices. Nevertheless, heat fluxes from ICs are increasing and air-cooling systems are not covering the necessity of high heat removal. This is why cooling systems using liquid cooling are now implemented as they improved significantly the cooling capacity, compactness and high performance with respect to air cooling devices. At this point, many advances have been investigated in micro-cooling systems for ICs.

Tuckerman et al. [2] were the first that introduced micro channels configuration to enhance the heat transfer coefficient between the substrate and the coolant. The heat transfer enhancement was based in the fact that heat transfer coefficient scales inversely with channel width. The main disadvantages of this configuration were the non-uniformity temperature distribution along the MC and the large pressure drops.

Another heat enhancement technique is the introduction of vortex generator (VG) within a MC to create a mixing fluid flow. VGs disturb the flow field, break the growth of the boundary layer, as well as provoke fluid swirling. Thus, there is a higher heat transfer enhancement between the fluid flow and the channels walls compared to a smooth MC. However, there is a notable increase of pressure drop, meaning higher power pump consumption. There are two types of VGs, transverse vortex generator (TVG) and longitudinal vortex generator (LVG). The main difference between them is the rotating axis, since TVGs have the axis rotating perpendicular to the flow direction while LVGs have the rotating axis parallel. However, LVGs have more effective effect than TVGs on the heat transfer performance [3].

Usually, vortex can be generated putting an object in the MC. Different motionless geometrical LVGs have been studied.

Chen et al. [4] experimentally investigated the effect of LVGs in MCs for different configurations of LVGs and with different MC aspect ratio, $\beta = \frac{H}{W}$, where H is the height and W the width of the MC. Results showed that MCs with a higher number of LVGs, an aspect ratio of 0.25 and a LVGs height of H/4 had better heat transfer enhancement between the fluid and MC walls. The increase in heat transfer coefficient (h) number in a MC with five pairs of LVGs was about 80% compared with a smooth channel as it is showed in Figure 1.

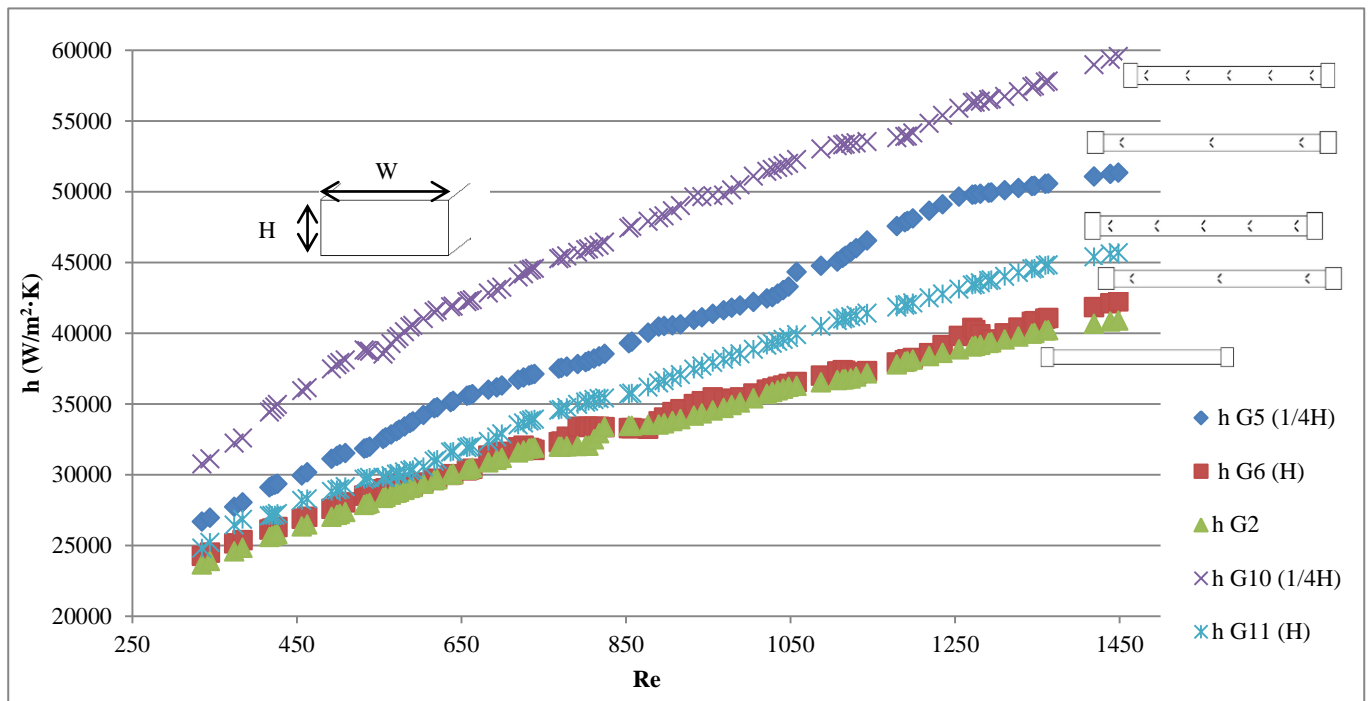


Figure 1: Heat transfer coefficient in function of Re number in whole configurations of MC with an aspect ratio of 0.25

Marschewski et al. [5] studied the improvement of heat transfer performance in MC for different herringbones structures and with a MC aspect ratio of 0.5. It was demonstrated that the best configuration was symmetric herringbones with half-height of the MC as it is shown in

Figure 2. The improvement in the heat transfer coefficient was 4 times bigger than in a smooth channel.

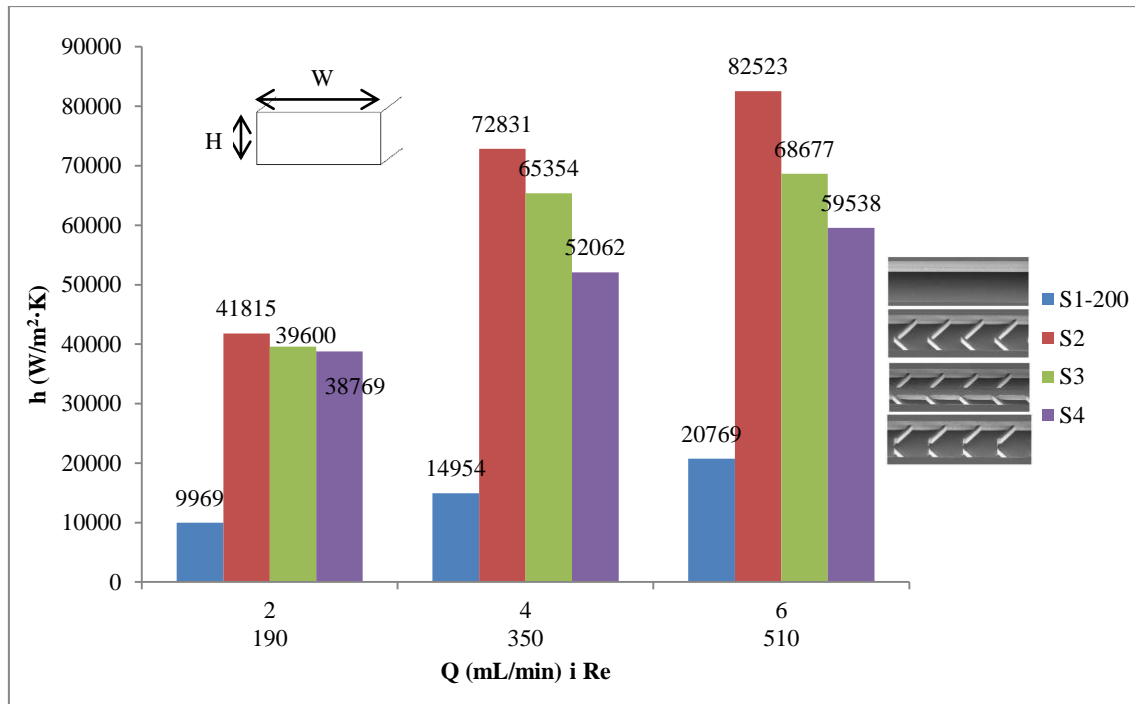


Figure 2: Heat transfer coefficient in MC with different herringbones configurations in function of flow rate and Re number.

Wang et al. [6] performed a study of a heat sink alternating ribs and grooves in its geometry to improve heat transfer performance between the coolant and the hot surface. It was demonstrated that the Nu number was higher as the relative height of ribs was higher too. Figure 3 shows the Nusselt number as function of Re number for all configurations. The approached increase of Nu number was 1.55 times that of smooth MC. However, when Re was low (around 200) there was not such increase.

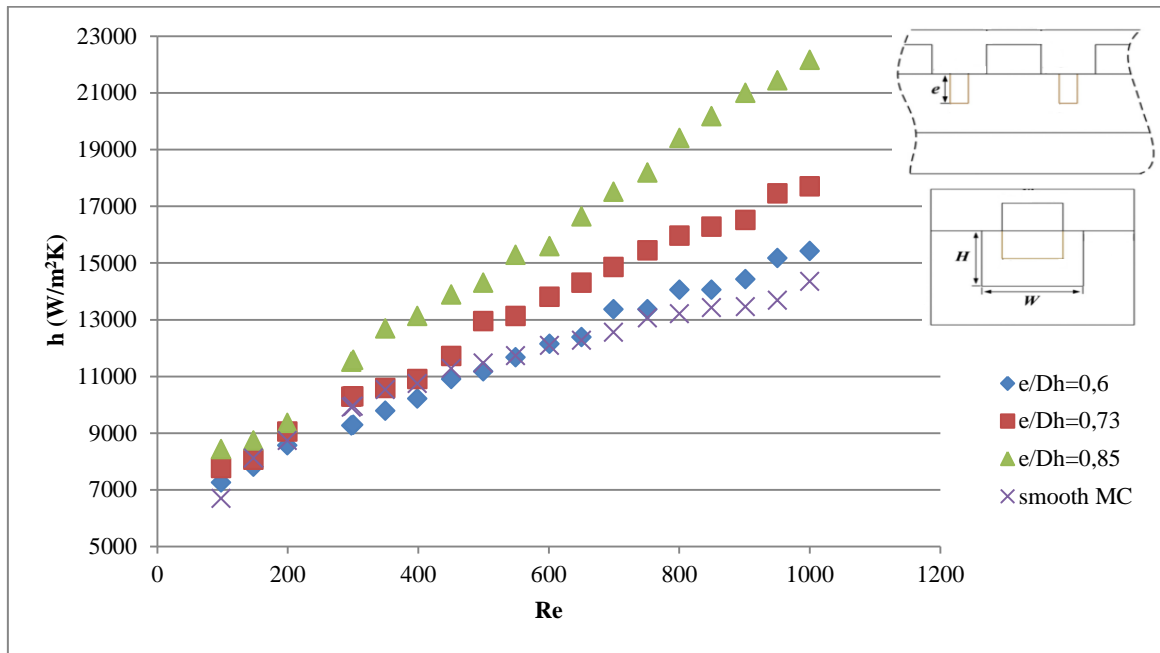


Figure 3: Heat transfer coefficient in function of Re number for different dimensions of a heat sink with an alternated ribs and grooves.

Riera et al. [7] developed a hybrid jet impingement/micro channel heat sink. The system was based in the entrance of fluid across a slot located in the symmetry plane of the device. Then, the coolant went along MC, which change their width throughout fluid path. In this case temperature difference between inlet and outlet was approximately 6°C, thus there was uniformity temperature distribution. In addition, thermal resistance coefficient was decreased compared to studies made at millimetre-scale in the same conditions [8]. The main disadvantage of this configuration was that the heat sink performance depended on the geometry. Therefore, it could not be used for time-dependent heat load distributions.

3.2. Self-adaptive fins

Once different cooling structures have been reviewed, the objective of this project is to found a novel generic solution to remove the heat, regardless its applications. That means the heat sink has to confront with different heat load scenario maintaining a uniform temperature distribution.

For this reason, smart materials have been studied in order to design self-adaptive structures within the micro channel.

First, bimetallic strips are evaluated. They are based in two materials, one with high coefficient of thermal expansion (CTE) and the other with low CTE. Then, two strips of each material are embedded each other. Therefore, when the bimetallic beam is heated, thermal energy is transformed to kinetic energy, because materials have a linear expansion.

Finally, SMAs are reviewed since they are materials that can be trained to have a self-adaptive performance.

3.2.1. Bimetallic beams clamped-clamped.

Figure 4 shows the geometry of a bimetallic beam clamped-clamped, that when it is at the micro scale can be also called microvalve.

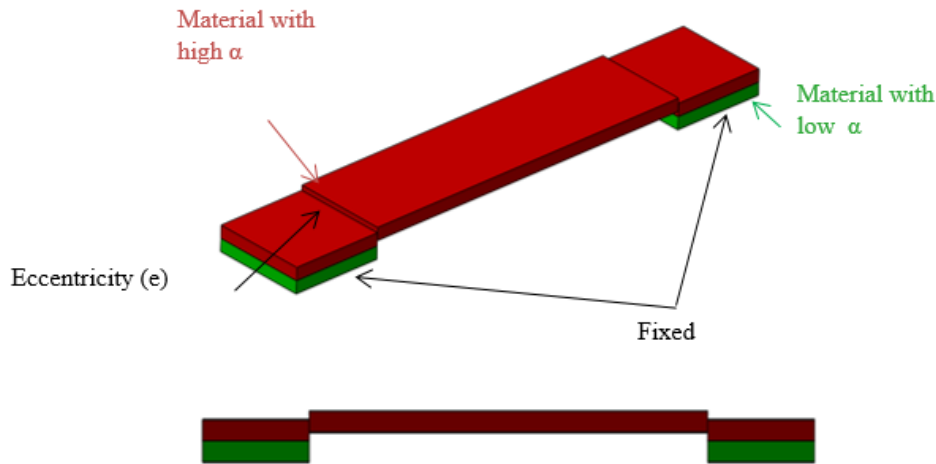


Figure 4: Geometry of a bimetallic beam clamped-clamped.

When the bimetallic strip is heated, there is thermal buckling. It occurs because the difference in CTE between both materials leads to an internal axial force. The beam is subject to compression and buckles at a critical load leading to deflection. The maximum deflection is reached in the middle of length's beam. As the temperature goes down, the bimetal beam returns to the initial position.

Arnaud et al. [9] studied experimentally the performance of an Al-Invar beam of dimensions $20 \times 2 \times 1\text{mm}^3$. The deflection reached when the beam was heated around 100°C was $206\mu\text{m}$. In this case, temperature hysteresis between buckling position and stable position was 5K. On the other hand, it was studied the theoretical performance of an Al-Si beam at the micro-scale ($100 \times 10 \times 15\mu\text{m}^3$) in same conditions. The result showed a deflection of $0,619\mu\text{m}$.

McCarthy et al. [10] studied the thermal buckling of eccentric micro-beam clamped-clamped made of nickel and deposited in a Si substrate. In this case, the micro-beam was made only with nickel and it can be named microvalve. The author evaluated different dimensions of beams. The highest deflection achieved was for a beam of $3000 \times 300 \times 60\mu\text{m}^3$ with an eccentricity of $0.75\mu\text{m}$ heated less than 100°C and its value was around $50\mu\text{m}$.

3.2.2. Bimetallic cantilevers.

Figure 5 shows the configuration of a general bimetallic cantilever.

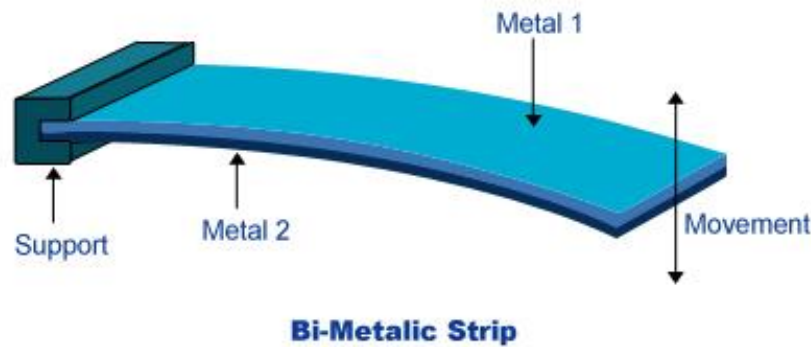


Figure 5: Geometry of a general bimetallic strip

It is based in two layers joined and one side of the beam embedded at a base. As before, one layer is made of a material with high CTE and the other one with low CTE. When the bimetallic strip is submitted to an increase of temperature, material with high CTE expands faster than the other one. Therefore, there is a combination of restrictions and movements that makes a deflection in the beam. Then, as temperature decreases the beam returns to its initial position.

Döring et al. [11] reported the design, fabrication and performance of a bimetallic cantilever submitted to electric power and cooled with forced convection using water as a coolant. The highest deflection was $44\mu\text{m}$ for a bimetal of $1 \times 1 \times 0.025\text{mm}^3$ and it was submitted to 1W power.

Chu et al. [12] developed an analytical model for predicting tip deflection of bimetallic cantilevers. The dimensions of the bimetallic cantilever material were $300 \times 100 \times 4\mu\text{m}^3$ for the material at the bottom and $300 \times 80 \times 1.8\mu\text{m}^3$ for the upper material. Bimetallic cantilever reached a tip deflection of $17\mu\text{m}$ with a temperature of 95°C .

3.2.3. Shape Memory Alloys (SMA)

SMA's are materials with two crystallographic phases and martensitic transformations that are reversible. They can be activated by thermal or mechanical loads. SMA's have two remarkable effects, shape memory effect and super-elasticity [13-15]:

Shape memory effect (SME) is explained as follows:

- The SMA has a parent austenite phase, which usually has a cubic symmetry crystal structure.
- When SMA is cooled, crystal structure has a reorientation to de-twinned martensite where there is a random orientation.
- In twinned martensite phase, SMA is easily deformed by an external load but always under elastic limit of the material.
- SMA's parent phase can be regained applying heat.

The process happens under a defined range of temperatures, creating an hysteresis loop.. This hysteresis depends on the chemical composition of the SMA, becoming the ones made of Nickel and Titanium (known as Nitinol) the most popular.

SMA's need to be trained, thus there are different processes to obtain the desired performance. The most trusting process is the two-way shape memory effect (TWSME). It consists in cooling SMA sample until the temperature where 100% martensitic phase is reached. Then, the sample is bended until the desired position. After that, heat is applied in the sample until the temperature where the SMA is 100% in austenitic phase is reached. The sample is thermally cycled from maximum temperature (austenitic phase) to minimum temperature (martensitic phase). The number of cycles is very important because when number of cycles increase the TWSME decrease.

Super-elasticity (SE) refers to the elastic response to an applied stress, caused by a phase transformation between the austenite and martensite phases of a SMA. Unlike SME, SE happens without a change of temperature. When a mechanical strain is imposed, there is a transformation from austenitic phase to de-twinned martensite phase, also called stress-induced martensite. As there is an unloading, the SMA returns to its original austenitic phase. In addition, it is important to apply a strain below plastic limit because the process could be irreversible.

The training process to obtain SE is based in repeatedly stress-inducing martensite within the super-elastic range. Like TWSME, the maximum temperature is the one that ensures the sample to be in its austenitic phase and the minimum temperature in the martensitic phase.

Although SMA's are very interesting to obtain self-adaptive structures, in this project they are not object of study.

4. Analytical study

Two mathematical models are implemented via Matlab. All the equations employed are defined below and the scripts are in the appendix of this project. The material with high CTE is Aluminium (Al), the material with low CTE is Silicon Dioxide (SiO₂) and the substrate is Silicon (Si). Table 1 shows the properties of materials.

Table 1: Materials properties.

Material	k (W/mK)	CTE (K ⁻¹)	E (N/m ²)
Al	235	23.1e-6	70e10
Si	148	3e-6	17e10
SiO ₂	1.3	0.6	70e10

Where k is the thermal conductivity, CTE is the coefficient of thermal expansion and E is the Young's Modulus.

4.1. Bimetallic beam clamped-clamped (Microvalve)

The study of the microvalve is based in three parts:

- The description of the whole model and their hypothesis
- The description of the analytical equations that define the performance of the microvalve as it is submitted to an increase of temperature.
- The implementation of the mathematical study in Matlab to obtain the optimal results and to know how the microvalve acts.

4.1.1. Model

McCarthy et al. [10] developed a numerical method to approach the performance of a clamped-clamped beam submitted to an increase of temperature. It was considered a pinned-pinned case to analyse the buckling effect and the results could be related with clamped-clamped beams as can be seen in Figure 6.

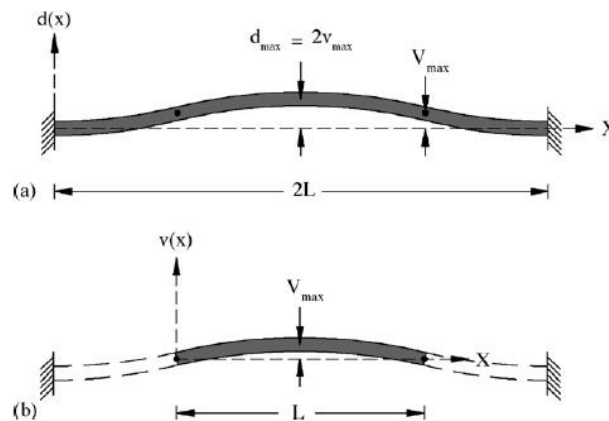


Figure 6: Simplification of clamped-clamped to pinned-pinned buckling: (a) clamped deflection $d(x)$ and (b) pinned deflection $v(x)$ from [10].

Equivalent loadings of pinned-pinned beams are described in Figure 7. The compressive force P could be applied out of the neutral axis, at some distance, to account the imperfections of the beam and the loading in the analysis. This load configuration was equivalent to a compressive load applied at the neutral axis and an additional moment, M_0 .

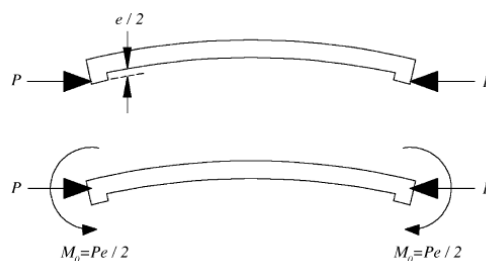


Figure 7: Loadings of pinned-pinned beams from [10].

The modelling approach can be seen in Figure 8.

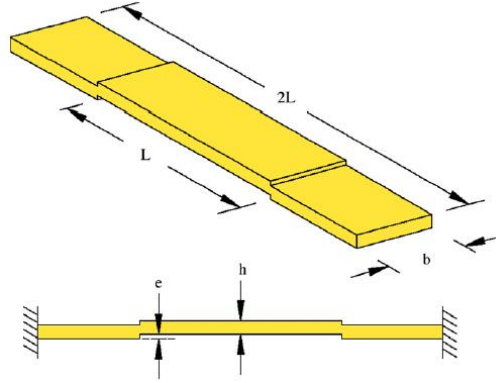


Figure 8: Beam studied, clamped-clamped beam with an eccentricity from [10].

The eccentricity parameter was important to ensure the appropriate direction of the buckling.

4.1.2. Analytical study

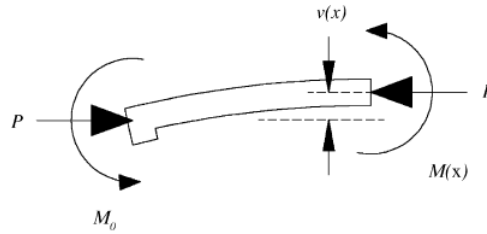


Figure 9: Free body diagram of pinned-pinned beams from [10].

An elastic analysis of the equivalent pinned-pinned beam was done following the free body diagram in Figure 9 and an elastic analysis.

$$EI \frac{d^2v}{dx^2} = M(x) = -M_0 - Pv = -P \left(\frac{e}{2} + v \right) \quad (1)$$

Where v was the pinned-pinned deflection, I beam moment of inertia, E Young's modulus and $M_0 = Pe/2$. Contour conditions were $v(0) = v(L) = 0$. So, equation 1 became:

$$\frac{d^2v}{dx^2} + \left(\frac{P}{EI} \right) v = -\frac{Pe}{2EI} \quad (2)$$

This has the following solution:

$$v(x) = \frac{e}{2} \left[\tan \left(\frac{L}{2} \sqrt{\frac{P}{EI}} \right) \sin \left(\sqrt{\frac{P}{EI}} x \right) + \cos \left(\sqrt{\frac{P}{EI}} x \right) - 1 \right] \quad (3)$$

Keeping in mind that the maximum deflection was reached in $L/2$, and there was a relation between pinned-pinned and clamped-clamped beam (Fig. 1), hence:

$$d_{MAX} = 2v \left(x = \frac{L}{2} \right) = e \left[\sec \left(\frac{L}{2} \sqrt{\frac{P}{EI}} \right) - 1 \right] \quad (4)$$

Equation 4 can be simplified:

$$P = E\Delta T\Delta\alpha A \quad (5)$$

$$d_{MAX} = e \left[\sec \left(\frac{L}{2h} \sqrt{12\Delta\alpha\Delta T} \right) - 1 \right] \quad (6)$$

Where ΔT was the average temperature rise, $\Delta\alpha$ was the difference in the coefficient of thermal expansion between the beam and the substrate and $A=bh$.

Once the dimensional parameters are defined, some non-dimensional parameters are defined as follows:

- The critical load, P_{cr} , was the force at which a theoretically perfect beam ($e=0$) will buckle:

$$P_{cr} = \frac{\pi^2 EI}{L^2} = \frac{\pi^2 E b h^3}{12 L^2} \quad (7)$$

- The critical temperature rise, ΔT_{cr} , was evaluated in Eq. 5 at the critical load.

$$\Delta T_{cr} = \frac{P_{cr}}{\Delta\alpha E b h} = \frac{1}{12\Delta\alpha} \left(\frac{\pi h}{L} \right)^2 \quad (8)$$

- Non-dimensional deflection (δ):

$$\delta = \frac{d_{MAX}}{h} \quad (9)$$

- Non-dimensional eccentricity (ε):

$$\varepsilon = \frac{e}{h} \quad (10)$$

- Non-dimensional axial load (η):

$$\eta = \frac{\pi}{2} \sqrt{\frac{P}{P_{cr}}} = \frac{L}{2} \sqrt{\frac{P}{EI}} \quad (11)$$

- Non-dimensional temperature (θ):

$$\theta = \frac{\Delta T}{\Delta T_{cr}} = \frac{12\Delta\alpha\Delta T}{\pi^2} \left(\frac{L}{2} \right)^2 \quad (12)$$

Finally, non-dimensional equations remained:

$$\delta = \varepsilon [\sec \eta - 1] \quad (13)$$

$$\theta = \left(\frac{2\eta}{\pi} \right)^2 \left[1 + \frac{3}{4} \varepsilon^2 \left\{ \frac{\tan \eta \cos 4\eta}{2\eta} + \tan^2 \eta \left(1 + \frac{\sin 4\eta}{4\eta} \right) + \left(1 - \frac{\sin 4\eta}{4\eta} \right) \right\} \right] \quad (14)$$

4.1.3. Analytical results

A numerical study has been carried out to obtain non-dimensional curves of a determined microvalve. This is the implementation of the equations developed in 4.1.2.

First, the maximum deformation is represented for different microvalve dimensions defined in Figure 8.

The microvalve is made of Aluminium embedded to a Si substrate.

Table 2 shows the inputs of the equation 6, which are the dimensional parameters, the increase of temperature and the CTE.

Table 2: Micro valve's dimensions used in the numerical study.

Dimension	Value
e (μm)	(0.5, 1, 2)
L (μm)	300
h (μm)	(1, 2, 3, 4, 5, 6)
w (μm)	50
ΔT (°C)	range[40,0.8,80]

Figure 10 shows the representation of the maximum deformation for different dimensions of the microvalve. Table 3 shows the legend of maximum deformation curves for all possible combinations between the eccentricity and the width of the microvalve.

Table 3: Eccentricity and width for each curve in figure 12.

dA	e=0.5 μm / h=1 μm	dJ	e=1 μm / h=4 μm
dB	e=0.5 μm / h=2 μm	dK	e=1 μm / h=5 μm
dC	e=0.5 μm / h=3 μm	dL	e=1 μm / h=6 μm
dD	e=0.5 μm / h=4 μm	dM	e=2 μm / h=1 μm
dE	e=0.5 μm / h=5 μm	dN	e=2 μm / h=2 μm
dF	e=0.5 μm / h=6 μm	dO	e=2 μm / h=3 μm
dG	e=1 μm / h=1 μm	dP	e=2 μm / h=4 μm
dH	e=1 μm / h=2 μm	dQ	e=2 μm / h=5 μm
dI	e=1 μm / h=3 μm	dR	e=2 μm / h=6 μm

Two mathematical models are implemented via Matlab. All the equations employed are defined below and the scripts are in the appendix of this project. The material with high CTE is Aluminium (Al), the material with low CTE is Silicon Dioxide (SiO₂) and the substrate is Silicon (Si). Table 1 shows the properties of materials.

Table 4: Materials properties.

Material	k (W/mK)	CTE (K^{-1})	E (N/m^2)
Al	235	23.1e-6	70e10
Si	148	3e-6	17e10
SiO ₂	1.3	0.6	70e10

Where k is the thermal conductivity, CTE is the coefficient of thermal expansion and E is the Young's Modulus.

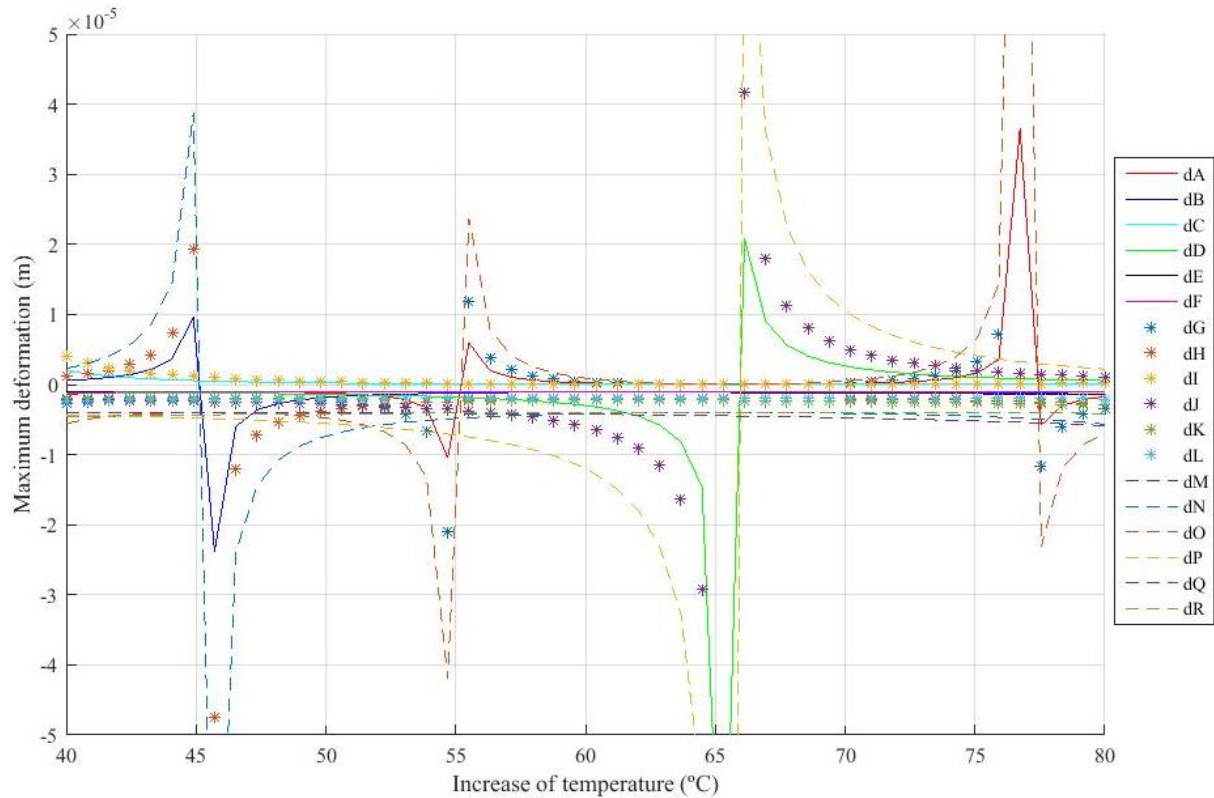


Figure 10: Maximum deformation in function of increase of temperature

It can be seen in figure 10 that each curve has a discontinuity, where the deformation tends to infinite. Therefore, this representation cannot be taken into account. For that reason, non-dimensional curves are plotted.

Non-dimensional curves are represented through equations 13 and 14. The calculation process is as follows:

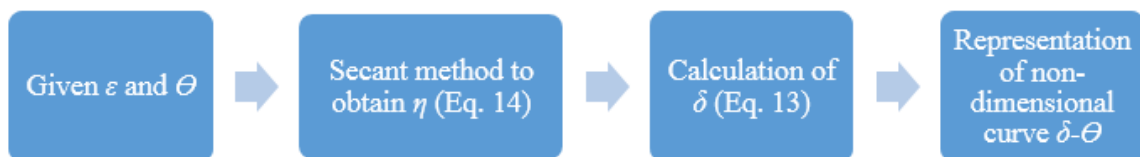


Figure 11 shows the flow chart of the secant method used.

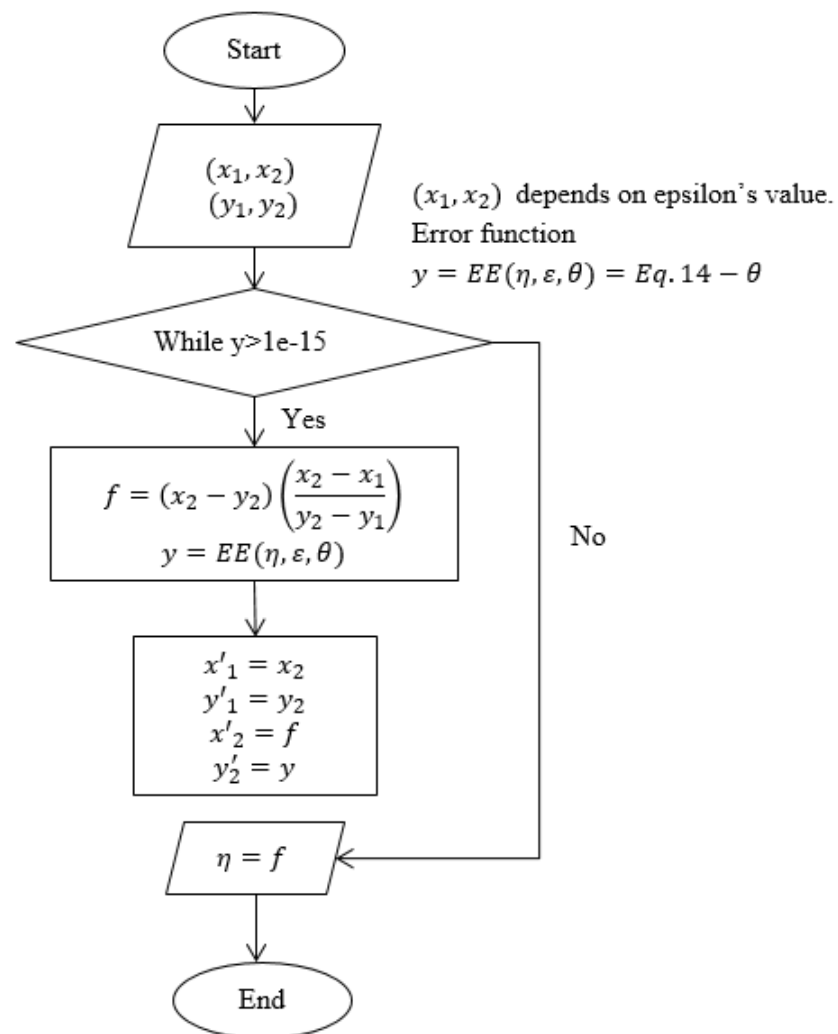


Figure 11: Flow chart of the secant method.

Finally, Figure 12 shows the non-dimensional curves for different ϵ .

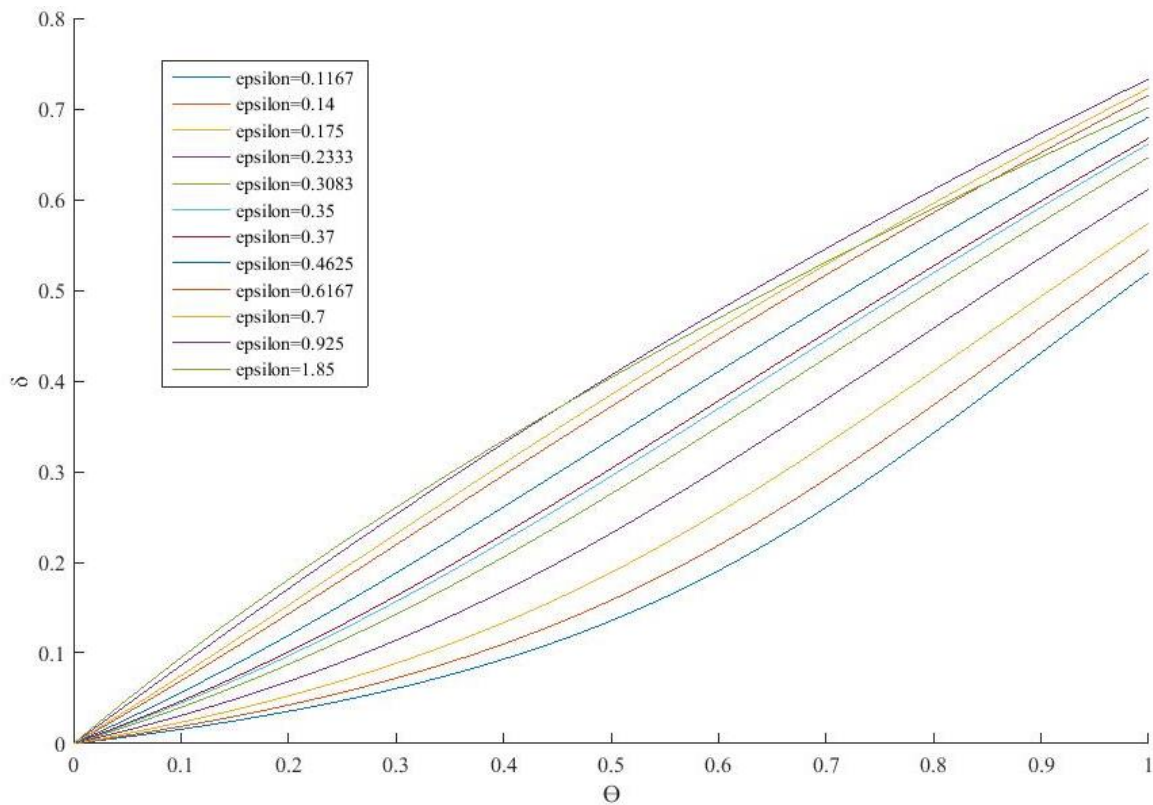


Figure 12: Non-dimensional curves of a microvalve in function of the non-dimensional temperature and for different values of ϵ .

Non-dimensional deflection increases as ϵ increases, too. Through the non-dimensional deflection is possible to know the deformation in the buckling effect for each value of epsilon and for a determined temperature.

4.2. Beam cantilever

The study of the bimetallic beam cantilever is based in three parts:

- The description of the whole model and their hypothesis.
- The development of the analytical equations that define the performance of the bimetallic strip as it is submitted to an increase of temperature.
- The implementation of the mathematical study in Matlab to obtain the optimal results and to know how the bimetallic strip performs.

4.2.1. Model

Figure 13 shows a bimetallic cantilever with all material and geometric parameters, where material 1 is the one with low CTE and material 2 is the one with high CTE.

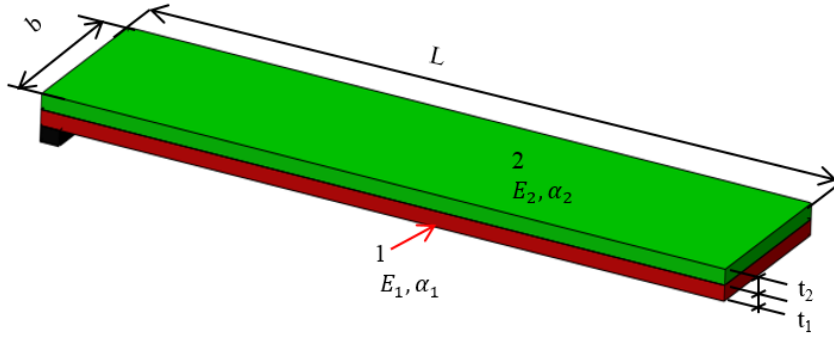


Figure 13: Bimetallic strip model with their characteristic parameters

4.2.2. Analytical study

Some assumptions are taken:

- (i) Sections 1 and 2 remain plane and rotate the same angle ($\theta_1 = \theta_2$).
- (ii) The strain of the top fibre of material 2 is the same of the bottom fibre of material 1 ($\varepsilon_{t1} = \varepsilon_{t2}$).
- (iii) An external moment M_0 is applied to the bimetallic section.

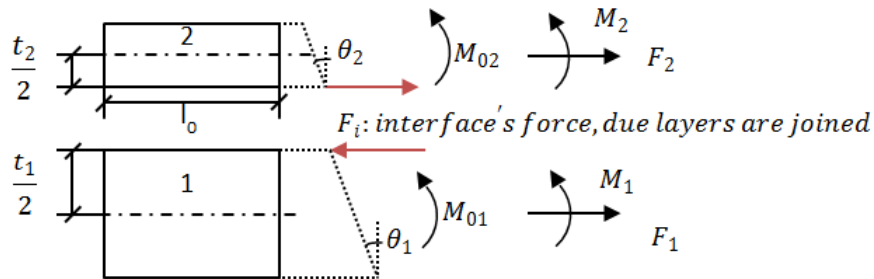


Figure 14: Free body diagram in sections 1 and 2 of a bimetallic strip

Forces and moments:

$$F_2 = F_i \quad (15)$$

$$M_2 = \frac{t_2}{2} F_i + M_{02} \quad (16)$$

$$F_1 = -F_i \quad (17)$$

$$M_1 = \frac{t_1}{2} F_i + M_{01} \quad (18)$$

Moment applied to the bimetallic section:

$$M_1 + M_2 = \frac{t_1 + t_2}{2} F_i + M_0 \quad (19)$$

$$\frac{M}{EI} = \frac{\theta}{l_0} \quad (20)$$

From Eq. 20, M for each layer:

$$M_1 = E_1 I_1 \frac{\theta_1}{l_0}; \quad M_2 = E_2 I_2 \frac{\theta_2}{l_0}$$

Where E is Young's modulus, I is moment of inertia and l_0 is the longitudinal increment of the beam.

Then Eq. 19 becomes:

$$E_1 I_1 \frac{\theta_1}{l_0} + E_2 I_2 \frac{\theta_2}{l_0} = \frac{t_1 + t_2}{2} F_i + M_0$$

Having in account the assumption $\theta_1 = \theta_2 = \theta$, F_i can be separate:

$$F_i = \frac{2}{t_1 + t_2} \left[(E_1 I_1 + E_2 I_2) \frac{\theta}{l_0} - M_0 \right] \quad (21)$$

The strain of top fibre of material 1 and bottom fibre of material 2 (effect of axial load + thermal load + moment load):

$$\varepsilon_t = \frac{F}{EA} + \alpha \Delta T - \frac{t}{2} \frac{M}{EI} \quad (22)$$

Replacing for each layer:

$$\varepsilon_{t1} = -\frac{F_i}{E_1 A_1} + \alpha_1 \Delta T - \frac{t_1}{2} \frac{\theta_1}{l_0} \quad (23)$$

$$\varepsilon_{t2} = \frac{F_i}{E_2 A_2} + \alpha_2 \Delta T + \frac{t_2}{2} \frac{\theta_2}{l_0} \quad (24)$$

Where α is the coefficient of thermal expansion of a determined material.

Imposing $\varepsilon_{t1} = \varepsilon_{t2}$ and $\theta_1 = \theta_2$:

$$-\frac{F_i}{E_1 A_1} + \alpha_1 \Delta T - \frac{t_1}{2} \frac{\theta_1}{l_0} = \frac{F_i}{E_2 A_2} + \alpha_2 \Delta T - \frac{t_2}{2} \frac{\theta_2}{l_0}$$

$$(\alpha_1 - \alpha_2) \Delta T = F_i \left(\frac{1}{E_1 A_1} + \frac{1}{E_2 A_2} \right) + \frac{t_1 + t_2}{2} \frac{\theta}{l_0}$$

Substituting F_i :

$$(\alpha_1 - \alpha_2) \Delta T = \left(\frac{2}{t_1 + t_2} \left[\left((E_1 I_1 + E_2 I_2) \frac{\theta}{l_0} - M_0 \right) \right] \right) \left(\frac{1}{E_1 A_1} + \frac{1}{E_2 A_2} \right) + \frac{t_1 + t_2}{2} \frac{\theta}{l_0}$$

$$M_0 = 0$$

$$\frac{\theta}{l_0} = \frac{(\alpha_1 - \alpha_2)\Delta T}{\frac{2}{t_1 + t_2}(E_1 I_1 + E_2 I_2) \left(\frac{1}{E_1 A_1} + \frac{1}{E_2 A_2} \right) + \frac{t_1 + t_2}{2}} \quad (23)$$

$$k_b = \frac{1}{r} = \frac{\theta}{l_0} \quad (24)$$

where r is the radius of curvature for each increment of l_0 along the bimetallic strip, so the deflection of the bimetallic strip submitted to an increase of temperature can be plotted.

4.2.3. Analytical results

The dimensions of bimetallic strip have been optimized to reach the highest tip deflection using the mathematical development made in 4.2.2. These are the width and the thickness, since the optimal length of the bimetallic strip is the largest one.

- Impact of width and thickness

Tip deflection has been calculated for different widths of each layer of the bimetallic strip and the other parameters constant. Table 1 and table 4 show the materials properties and the dimensions of the bimetallic strip, respectively.

Table 5: Dimensions of bimetallic strip in the study of impact width.

b_1 (μm)	range [10,0.45,100]
b_2 (μm)	range [10,0.45,100]
t_1 (μm)	0.5
t_2 (μm)	0.5
L (μm)	300
ΔT (°C)	60

The curvature is calculated following the equation 23 and it is considered constant. Tip deflection is approached with equation 24 [12].

$$d = \frac{k_b L^2}{2} \quad (25)$$

Where k_b is the curvature of the bimetallic strip, L is the length of the bimetallic beam and d is the tip deflection reached.

Figure 15 shows the optimal width for both Al and SiO₂ layers of bimetallic strip.

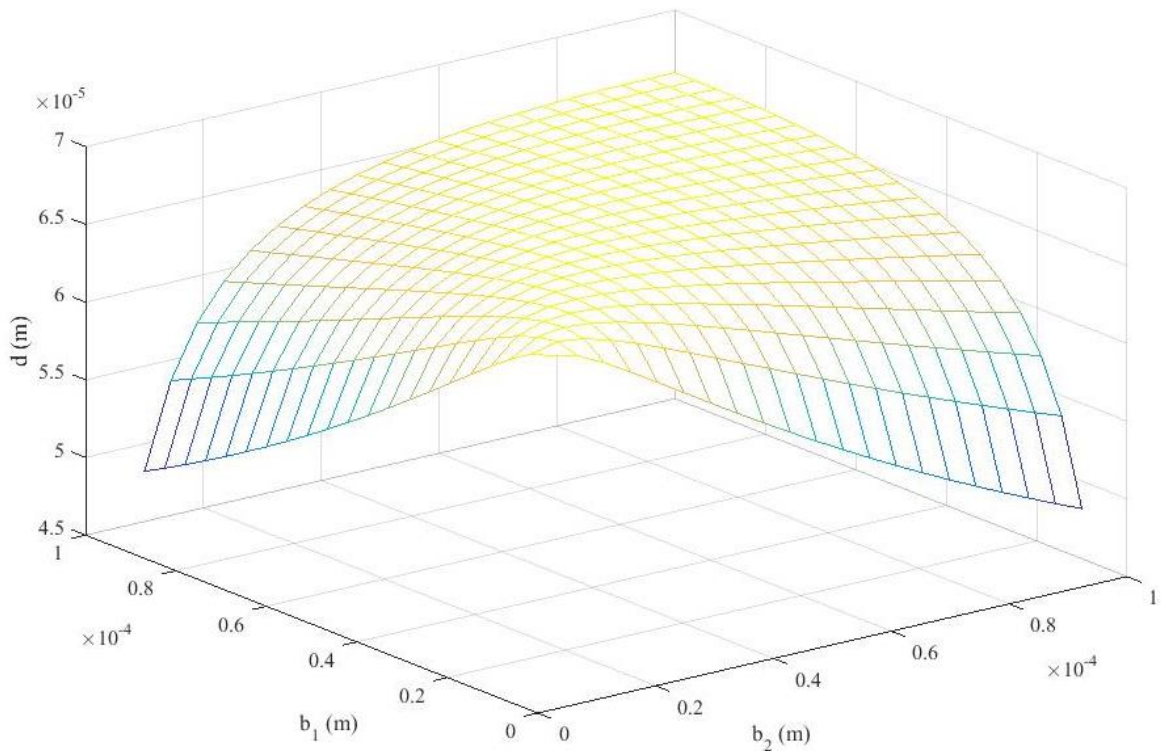


Figure 15: Impact of width in tip deflection of the bimetallic cantilever.

The result shows that the width of each layer should be equal to reach the highest tip deflection.

Now, the changing parameters are the thickness of both layers and the other parameters remain constant. Table 5 shows the values for each parameter.

Table 6: Dimensions of bimetallic strip in the study of impact thickness.

b_1 (μm)	50
b_2 (μm)	50
t_1 (μm)	range [0.5,0.1,2.5]
t_2 (μm)	range [0.5,0.1,2.5]
L (μm)	300
ΔT ($^{\circ}\text{C}$)	60

Figure 16 shows the optimal values of thickness.

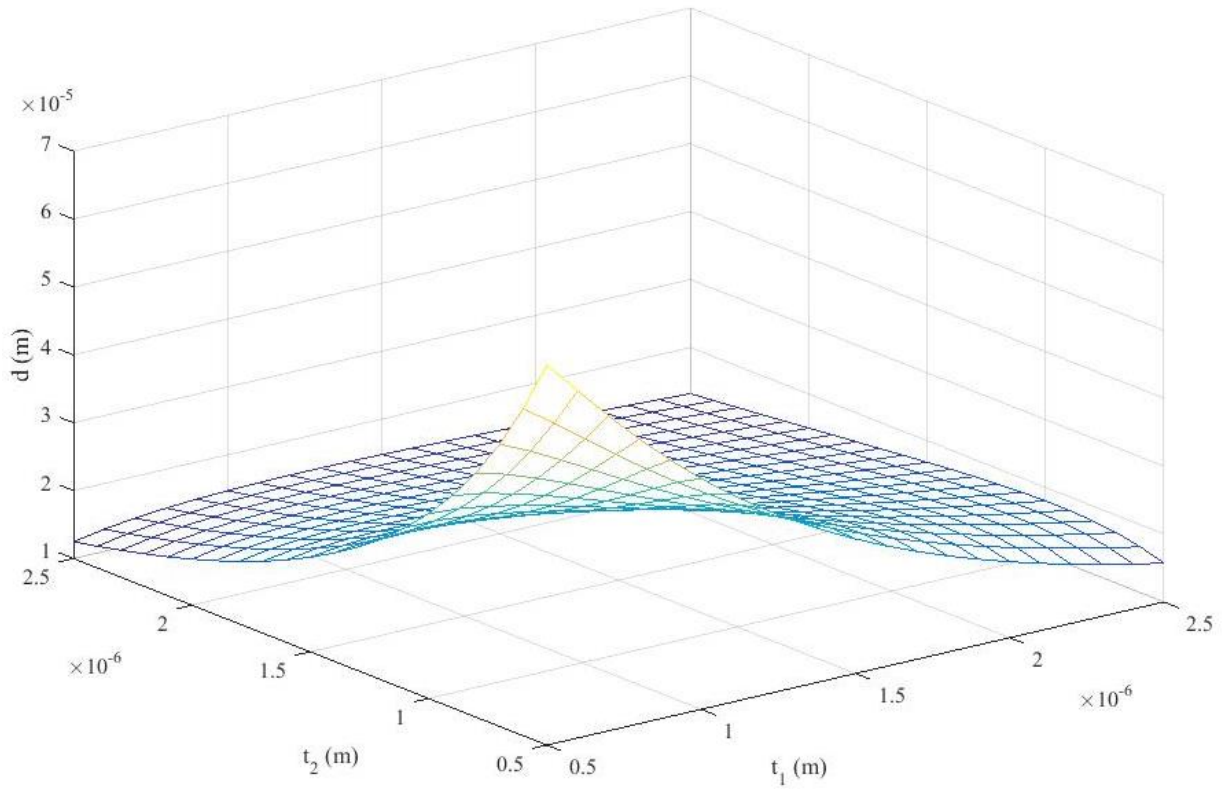


Figure 16: Impact of thickness in tip deflection of the bimetallic cantilever.

Optimal thickness is the smallest value of the whole range, $0.5\mu\text{m}$. In addition, $t_1 = t_2$.

- Deflection of bimetallic cantilever

The study has been made for three heat transfer coefficient, $20000 \frac{W}{m^2K}$, $10000 \frac{W}{m^2K}$ and $50000 \frac{W}{m^2K}$. The temperature along the fin is not constant, so it is calculated through equation 26 [16].

$$T(x) = (T_b - T_{fluid}) \frac{\cosh(m(L-x)) + \left(\frac{h}{mk}\right) \sinh(m(L-x))}{\cosh(mL) + \left(\frac{h}{mk}\right) \sinh(mL)} + T_{fluid} \quad (26)$$

Where T_b is temperature at the base, T_{fluid} is the temperature of the fluid, L is the longitude of the bimetallic strip, x the position along the bimetallic strip, k is thermal conductivity, h is the heat transfer coefficient between the bimetallic strip and the fluid and $m = \sqrt{\frac{hP}{kA_c}}$ (P is the perimeter of cross section and A_c is the cross area of the bimetallic strip).

The angle of curvature is calculated for a small increment ($3 \mu\text{m}$) along the bimetallic beam through equation 23. The dimensional values considered are listed in table 6.

Table 7: Given values for numerical study of bimetallic deflection

b_1 (μm)	100
b_2 (μm)	100
t_1 (μm)	0.5
t_2 (μm)	0.5
L (μm)	300
T_b ($^{\circ}\text{C}$)	70
T_{fluid} ($^{\circ}\text{C}$)	25
h ($\frac{\text{W}}{\text{m}^2\text{K}}$)	(2000, 10000, 50000)

Once the angle of curvature of an increment is calculated, it accumulates to the previous. Then, the vertical component is founded with a trigonometrically relation. This component is the maximum height reached for the bimetallic strip. Figure 17 shows the profile of the bimetallic strip with the effect of heat transfer and non-constant temperature along the fin.

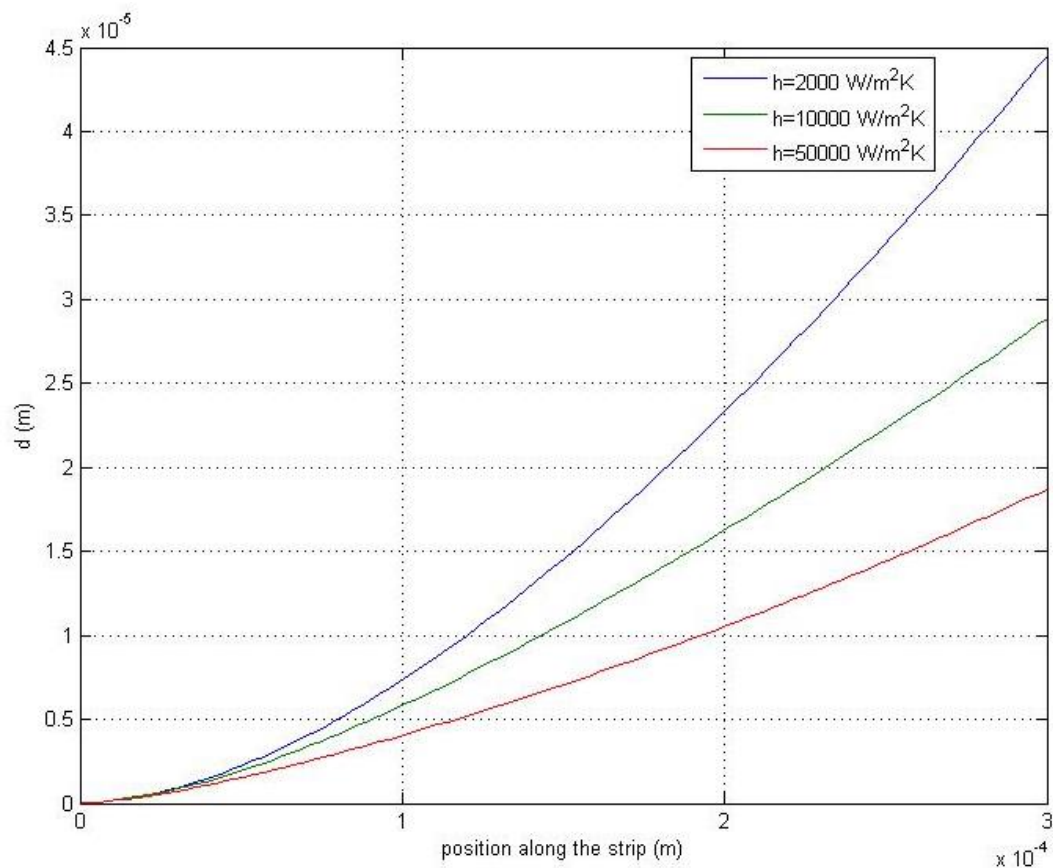


Figure 17: Profile of the bimetallic strip for given dimensions in table 6 for different heat transfer coefficient and non-constant temperature along the bimetallic strip.

The highest tip deflection is reached for the lowest h .

5. Numerical study of micro actuators

Different self-adaptive structures are studied via COMSOL Multiphysics to obtain the optimal dimensions that make the tip deflection the highest.

5.1. Study of the mesh sensibility

Since the program used to do the simulations is COMSOL Multiphysics, a study of the mesh sensibility is done in order to obtain the greatest precision with an optimal modelling. The design chose to do this study is the bimetallic strip with one side embedded at the substrate. The material with low CTE is SiO₂ and with high CTE is Al, as in the previous cases. Table 7 shows the dimension of the design simulated with different structure mesh.

Table 8: Dimensions of the modelling used to study the mesh sensibility

b (μm)	50
L (μm)	300
t₁ (μm)	5
t₂ (μm)	5

The different meshes used are the normal, fine, finer and extra finer sizes. The value measured is the tip deflection of the bimetallic strip when the same increase of temperature is applied at the Si substrate. Table 8 shows the result for each mesh.

Table 9: Comparison between the results obtained with different mesh size

Mesh size	Tip deflection (μm)
Normal	9.4865
Fine	9.4782
Finer	9.4728
Extra fine	9.4721

There is a big difference between the normal and the fine meshes. However, fin, finer and extra finer meshes have the same value until the second decimal. Finally, the mesh chosen is the **finer** one, since it has a similar result than the extra fine mesh. But also, it has half points to study so the time required in the simulation is lower.

5.2. Buckling effect: Microvalve

The microvalve is based in a clamped-clamped beam. There is an eccentricity between supports and the beam (Fig. 18).

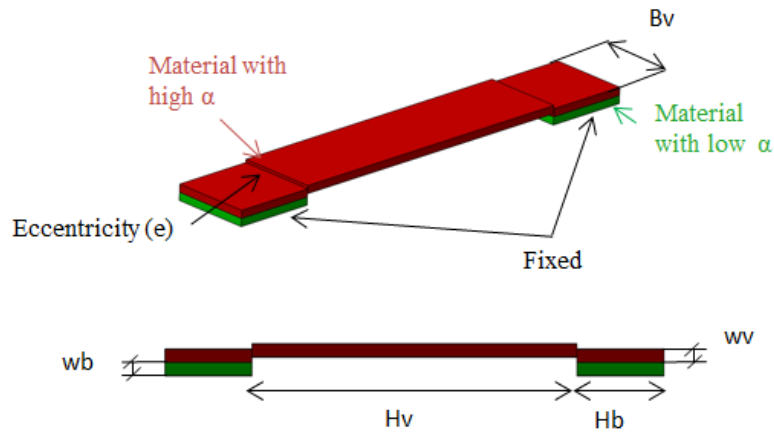


Figure 18: Description and design parameters of the microvalve.

A microvalve is designed to analyse the effect of thermal expansion and the buckling effect. Table 9 shows the dimensions chosen.

Table 10: Dimensions of the microvalve.

Constant parameters	
ΔT (°C)	60
w_b (μm)	5
w_v (μm)	5
e (μm)	2
Variable parameters	
B_v (μm)	range [50,50,100]
H_v (μm)	range [100,100,300]
H_b (μm)	range [20,20,160]

The constant parameters are the thickness and the eccentricity. The dependence of the deflection in function of the thickness parameter is known from the results obtained in the bimetallic cantilever fin study (point 5.2). Therefore, as the thickness decreases the deflection increases. Moreover, the deflection increases as the eccentricity increases too.

The influence of the other dimensional parameters on the maximum deflection (d_{MAX}).is studied through a parametric study. The result is composed of 75 combinations and these relations are shown as follows:

- $H_b - d_{MAX}$

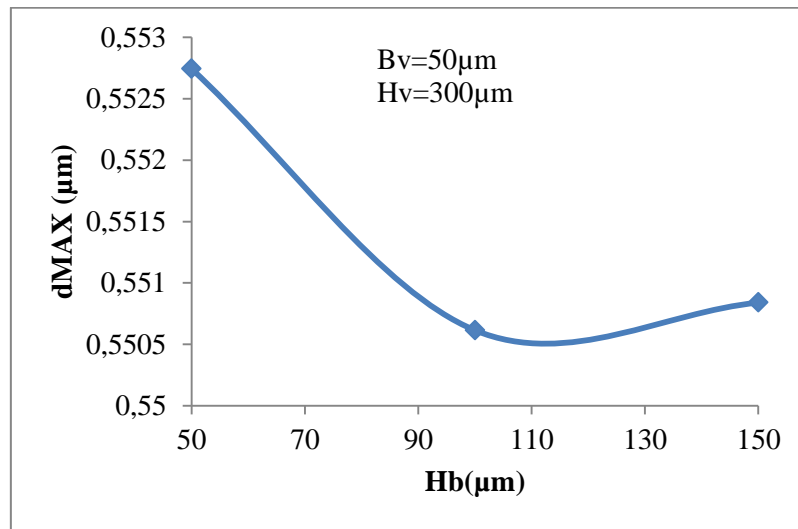


Figure 19: Relation between H_b and d_{MAX} of the microvalve, when $B_v = 50\mu m$ and $H_v = 300\mu m$.

Figure 20 shows there is no big differences when H_b change, but higher tip deflection is reached when $H_b = 50\mu m$.

- $H_v - d_{MAX}$

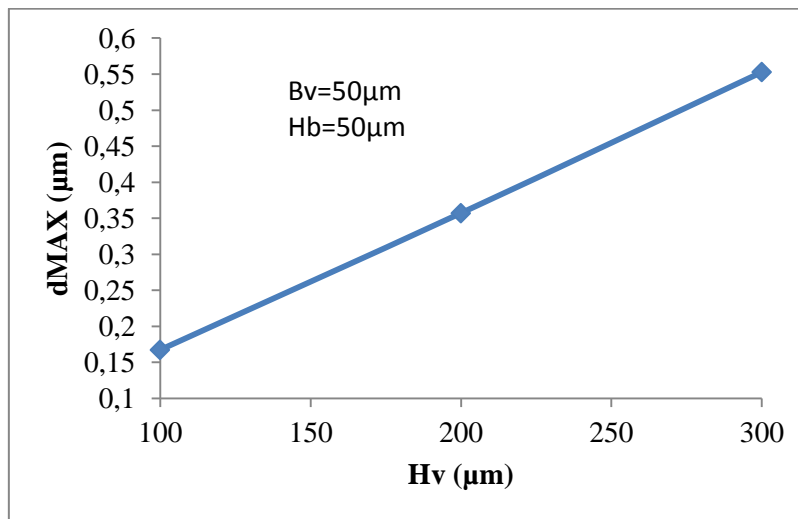


Figure 20: Relation between H_v and d_{MAX} of the microvalve, when $B_v = 50\mu m$ and $H_b = 50\mu m$.

It can be seen that d_{MAX} is higher as H_v increases.

- $B_v - d_{MAX}$

Table 11: Relation between B_v and d_{MAX} of the microvalve, when $H_b = 50\mu m$ and $H_v = 300\mu m$.

$B_v (\mu m)$	Tip deflection (μm)
50	0.553
100	0.549

It can be seen that d_{MAX} does not present big changes, so B_v is not an influent parameter. The parameter that influences more in the maximum deflection is the length of the middle strip in the microvalve, so it is interesting a high value to achieve the best result.

Finally, maximum tip deflection is reached with $B_v = 50\mu\text{m}$, $H_v = 300\mu\text{m}$ and $H_b = 50\mu\text{m}$ and its value is **0,553 μm** .

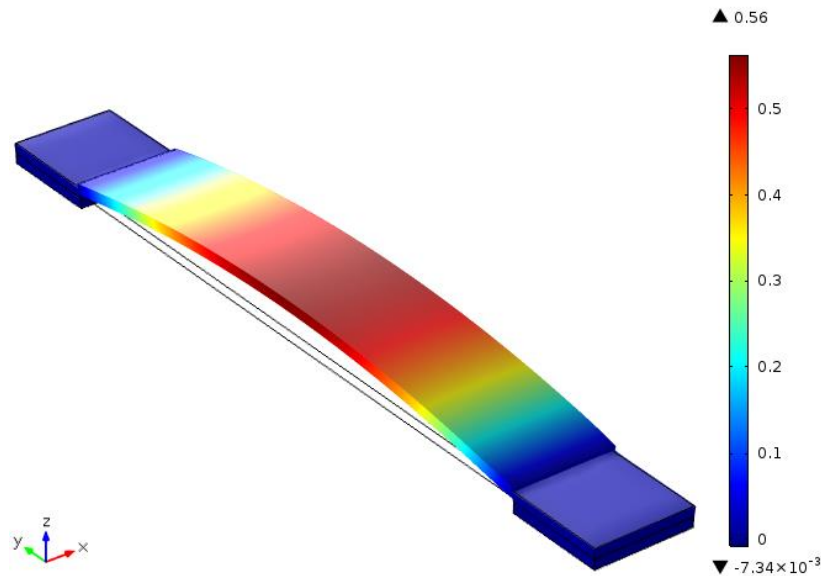


Figure 21: Maximum deflection of the microvalve reached when $\Delta T = 60\text{K}$.

5.3. Deflection effect: Bimetallic cantilever fin

A bimetallic cantilever embedded in one side to a Si substrate is designed. The top material of the bimetallic fin is SiO_2 with high CTE and the bottom material is Aluminium, with low CTE.

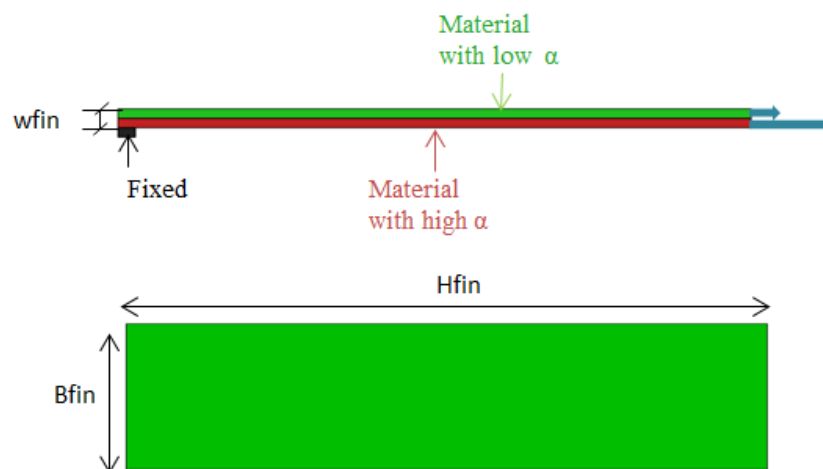


Figure 22: Description and design parameters of the bimetallic strip.

The parameters of the bimetallic strip design are described in figure 18. In order to optimize these parameters to obtain the greatest tip deflection, a parametric study is done. Table 11 shows the constant and variable values of the parameters.

Table 12: Dimensions of bimetallic strip.

Constant parameters	
ΔT (K)	60
Variable parameters	
Hfin (μm)	range [100,50,300]
Bfin (μm)	range [10,22.5,100]
wfin (μm)	range [1,1,5]

The result is composed of 125 combinations and the following relations have been made to study the impact of design parameters in the tip deflection.

- wfin – tip deflection:

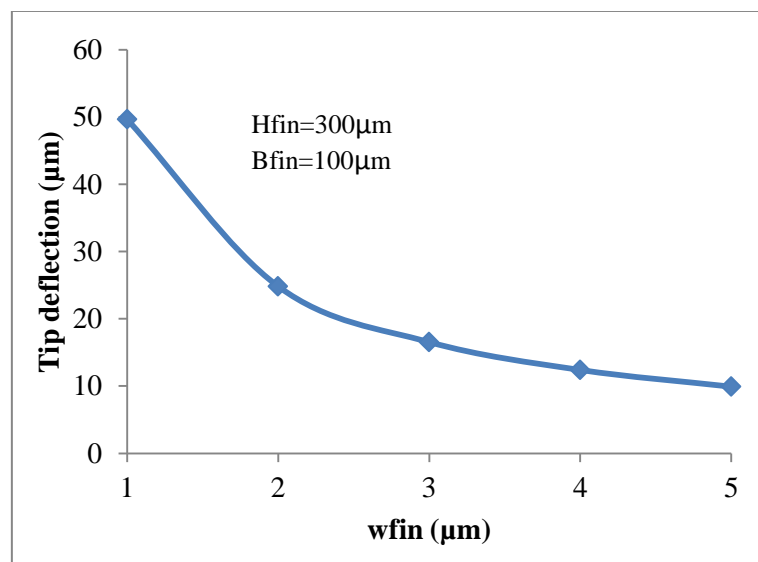


Figure 23: Relation between thickness and tip deflection of the bimetallic strip, when Hfin=300 μm and Bfin=100 μm .

The tip deflection decreases as thickness increase.

- H_{fin} – tip deflection:

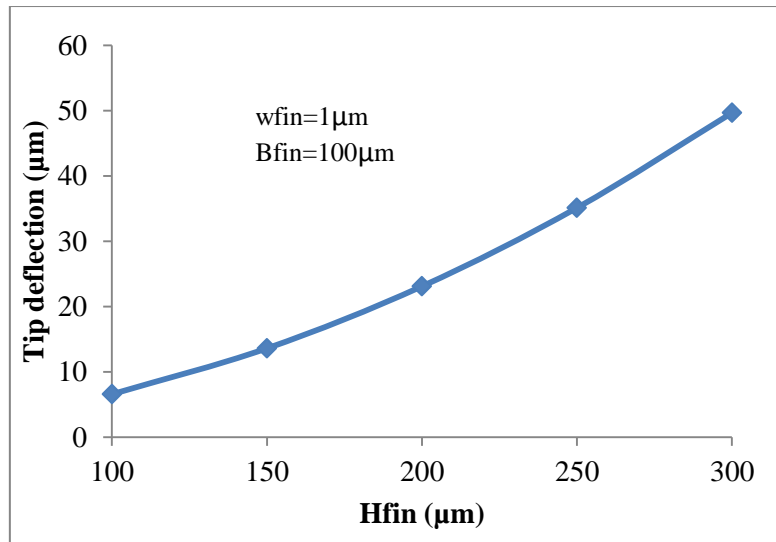


Figure 24: Relation between height and tip deflection of the bimetallic strip, when $B_{fin}=100\mu\text{m}$ and $w_{fin}=1\mu\text{m}$.

The tip deflection rises as the fin's height is higher.

- Width – tip deflection:

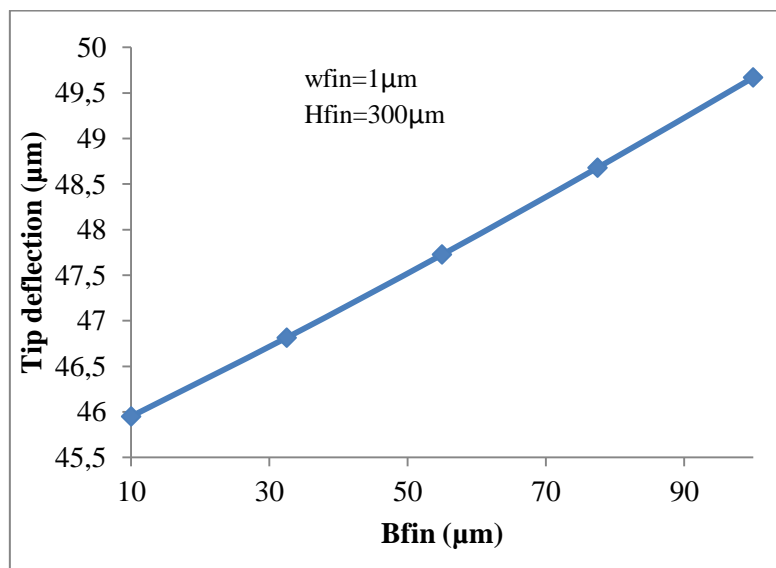


Figure 25: Relation between width and tip deflection of the bimetallic strip, when $H_{fin}=300\mu\text{m}$ and $w_{fin}=1\mu\text{m}$.

The tip deflection has a slightly increase as width rises.

To conclude, it can be seen that thickness and height have a bigger influence than width in the tip deflection of bimetallic beam. Hence, thickness has to be as small as possible and height has to be as big as possible to reach higher tip deflection.

The parametric study shows that the maximum tip deflection is reached with $B_{fin} = 100\mu\text{m}$, $H_{fin} = 300\mu\text{m}$ and $w_{fin} = 1\mu\text{m}$ and its value is **49,668 μm** .

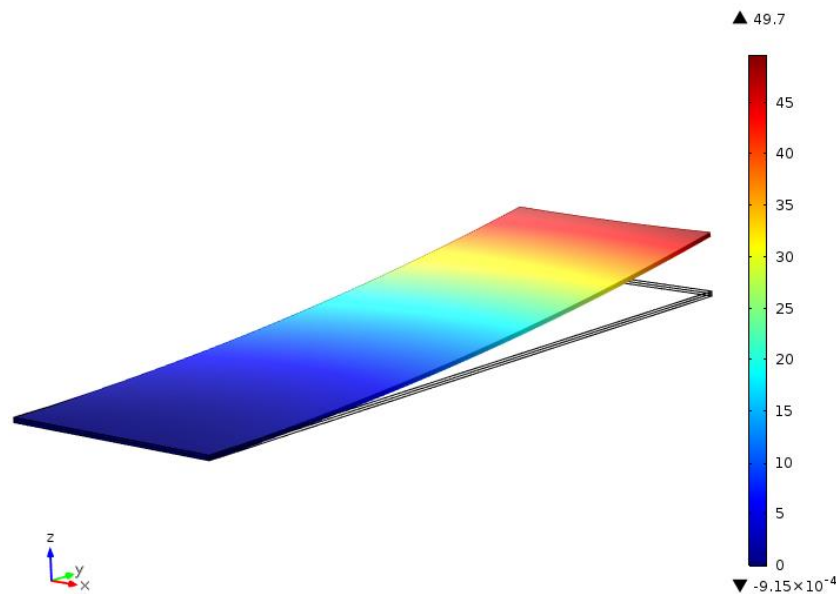


Figure 26: Maximum tip deflection of bimetallic strip reached when $\Delta T = 60\text{K}$.

5.4. Combination between deflection and buckling effect

Once buckling and deflection effect have been studied separated, it is interesting to combine both effects in order to obtain higher tip deflection. Figure 21 shows a design with a bimetallic strip and a microvalve.

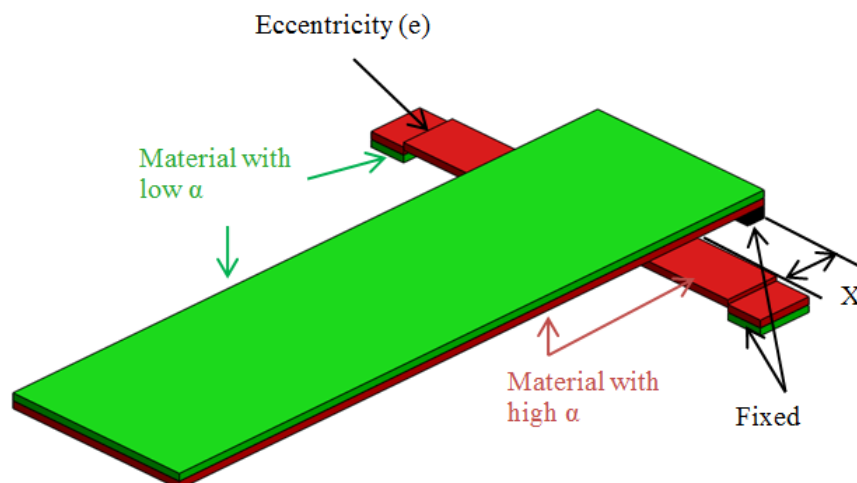


Figure 27: Description and design parameters of combined model microvalve + bimetal strip.

As optimal values of the bimetallic strip and the microvalve have been obtained previously, it is interesting to optimize the position X. Thus, microvalve situated at the bottom of the bimetal strip makes a lever effect. Table 12 shows the dimensions of this model.

Table 13: Dimensions of design model 8.

Constant parameters	
ΔT (K)	60
H_{fin} (μm)	300
B_{fin} (μm)	100
w_{fin} (μm)	1
B_v (μm)	20
H_v (μm)	300
H_b (μm)	50
w_b (μm)	1
e (μm)	0,5

The simulation has been done for different position of the microvalve in a range from 5 to 100 microns. Figure 29 shows the influence of the change of X in the tip deflection of the fin.

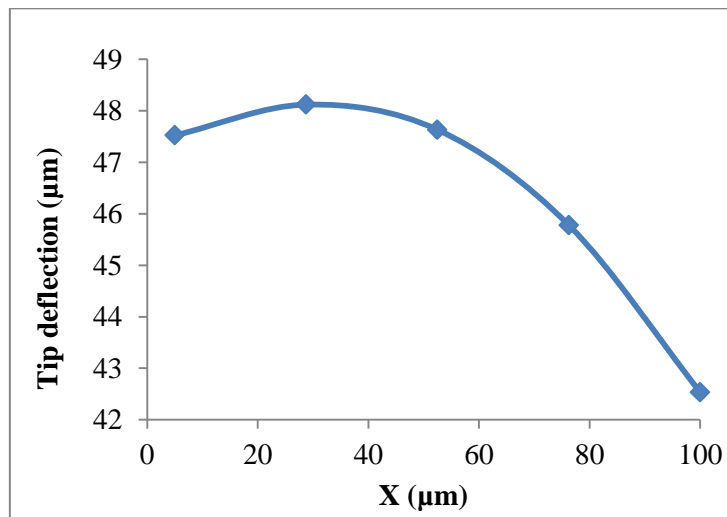


Figure 28: Relation between X and tip deflection of bimetallic strip + microvalve.

The best result is reached in $X=28.75\mu m$, where tip deflection is $48.119\mu m$.

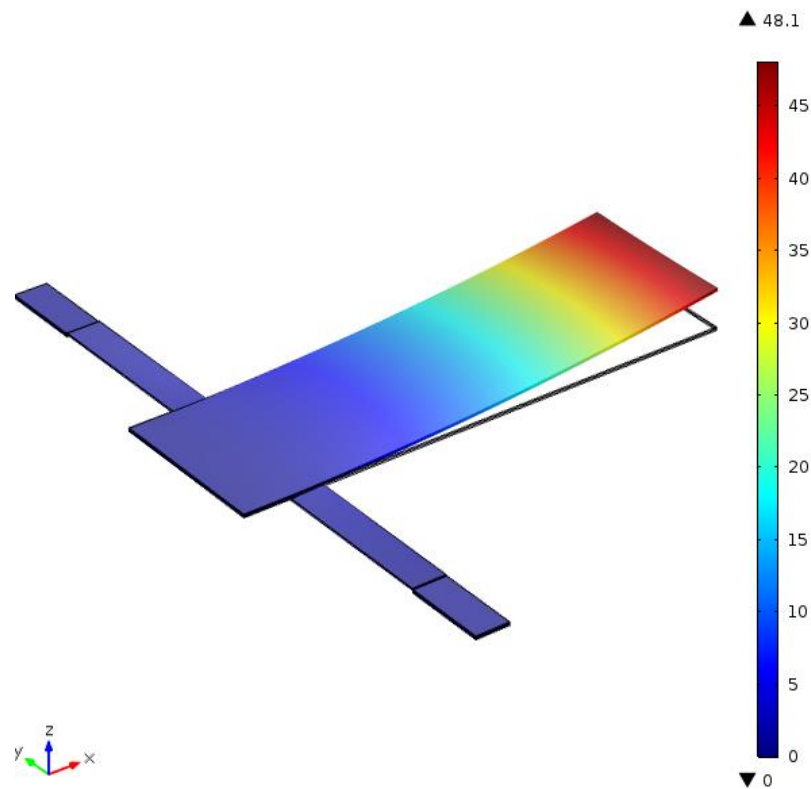


Figure 29: Maximum tip deflection reached when $\Delta T=60K$ and the bimetallic strip is on the microvalve.

On the other hand, a second design derived to the last one is made. Now the bimetallic strip and the microvalve are joined as we can see in figure 24. The microvalve is made of Al and it is joined with the layer of Al of the bimetal strip, and top layer of bimetal beam is made of SiO_2 . Restrictions of movement are putted in both sides of the microvalve.

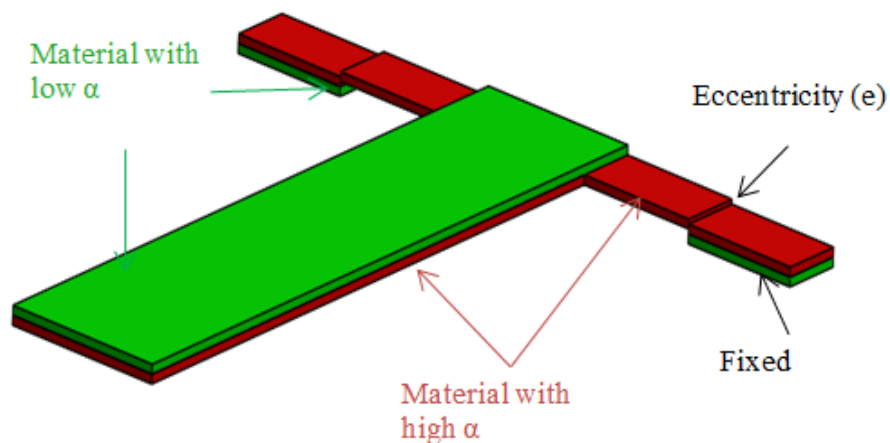


Figure 30: Description and design parameters of combined model microvalve joined to a bimetal strip.

Table 13 shows the dimensions of the model.

Table 14: Dimensions of design 9.

Constant parameters	
ΔT (°C)	60
L (μm)	300
w (μm)	50
H (μm) (each layer)	1
L_{valv} (μm)	100
H_{valv} (μm)	1
W_{valv} (μm)	30
e (μm)	0.5

The simulation is made for different position of the microvalve in a range from 0 to 100 microns.

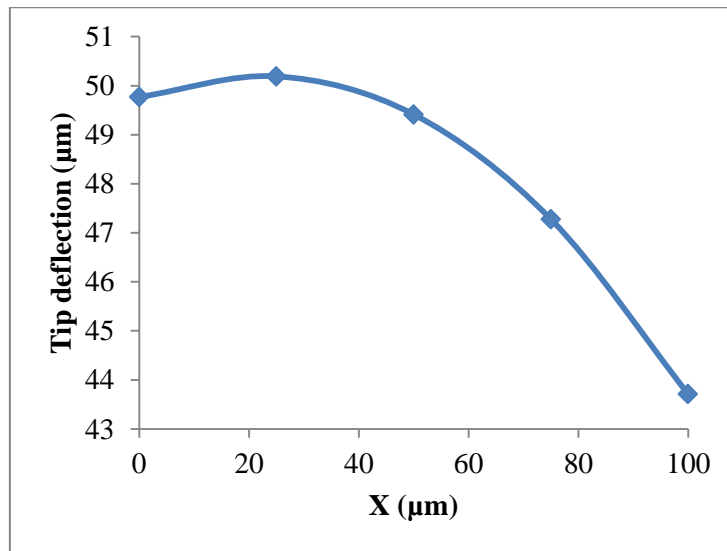


Figure 31: Relation between X and tip deflection of bimetallic strip joined with a microvalve.

It can be seen that the best result is reached in $X=25\mu\text{m}$, where tip deflection is $50.191\mu\text{m}$.

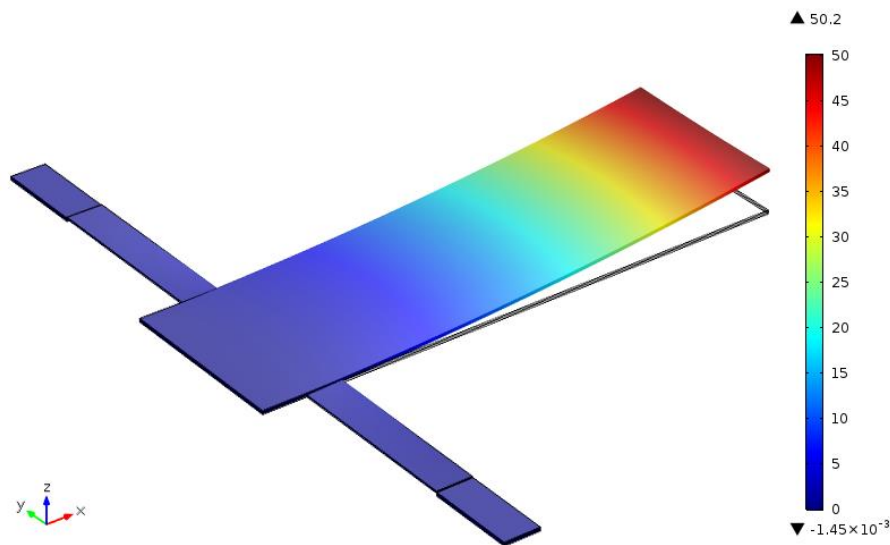


Figure 32: Maximum tip deflection reached when $\Delta T=60K$ and the bimetallic strip joined to the microvalve.

To conclude, if both lever models are compared it is preferable the last design where the bimetallic strip is joined with the microvalve, because tip deflection is bigger.

5.5. Triangular fins

In the wake of bimetallic effect, some configurations have been simulated to approach the performance of these triangular fins.

5.5.1. Model 1

The first option is to combine materials as it is shown in figure 33. Central path and triangular part of the fin are made of aluminium and both sides are made of SiO_2 . There is a restriction of movement in the three paths.

Second option is based on contrary combination of materials, as it is seen in fig 34. Only the central path is made of aluminium and the remainder is made of SiO_2

The performance expected is based in thermal expansion when temperature increases at the Si base. Then, material with high CTE has a bigger linear expansion than material with low CTE. Since paths are embedded at the Si substrate, different forces are induced. This combination of forces produces a deflection in the fin.

A parametric study for both options has been done. In triangular fins is difficult to obtain a mathematical model due to shape and the ignorance of material's displacement when they are submitted to an increase of temperature.

a) Model 1a

Figure 33 shows the triangular design with one combination of materials, it is called model 1a.

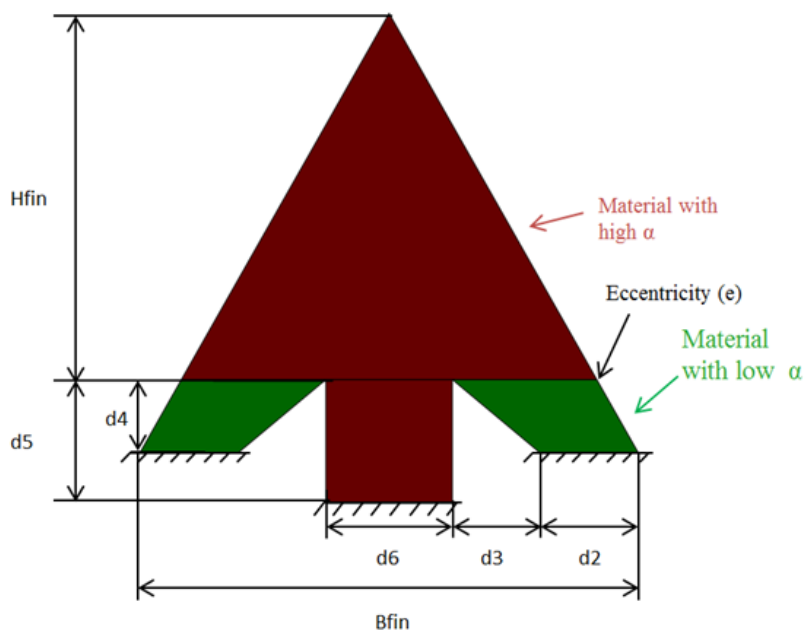


Figure 33: Description and parameters of triangular fin model 1a.

As before, table 14 shows the constant and variable dimensions.

Table 15: Dimensions of triangular fin model 1a.

Constant parameters	
ΔT (K)	60
e (μm)	2
w_{fin} (μm)	5
H_{fin} (μm)	300
T_{ref} (K)	293,15
d_4 (μm)	50
Variable parameters	
d_2 (μm)	range [20,20,100]
d_3 (μm)	range [10,10,50]
d_5 (μm)	range [20,20,100]
d_6 (μm)	50 / 100

The simulation has done 125 combinations. The influence of variable parameters has been evaluated when $d_6 = 50\mu\text{m}$ and $100\mu\text{m}$, respectively.

- Influence of parameter d_2 :

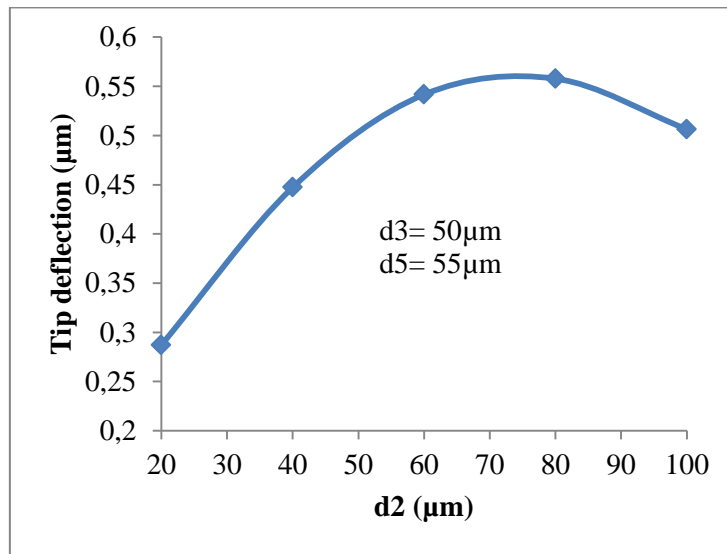


Figure 34: Relation between parameter d_2 and tip deflection of the fin model 1a, when $d_3=50\mu\text{m}$, $d_5=55\mu\text{m}$ and $d_6=50\mu\text{m}$.

Tip deflection increases until $d_2=80\mu\text{m}$, where there is a maximum.

- Influence of parameter d_3 :

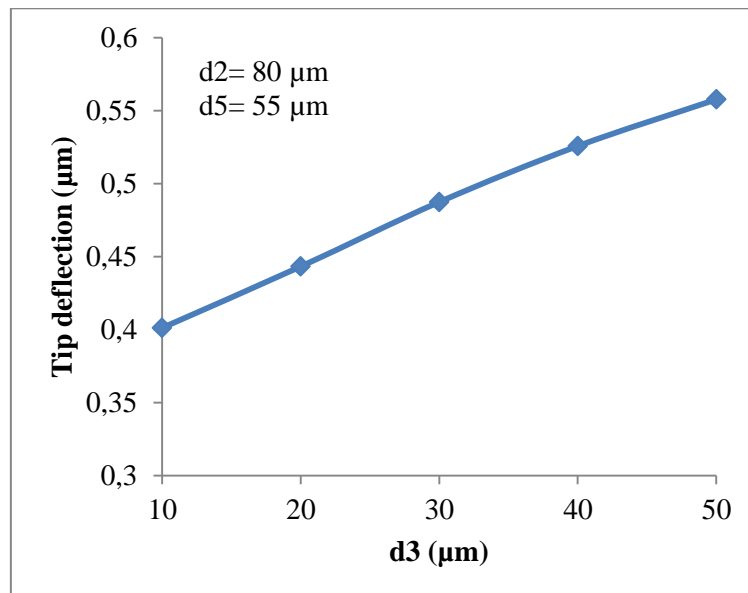


Figure 35: Relation between parameter d_3 and tip deflection of the fin model 1a, when $d_2=80\mu\text{m}$, $d_5=55\mu\text{m}$ and $d_6=50\mu\text{m}$.

Parameter d_3 influence approximately proportional to the tip deflection, thus tip deflection increases when d_3 rises.

- Influence of parameter d_5 :

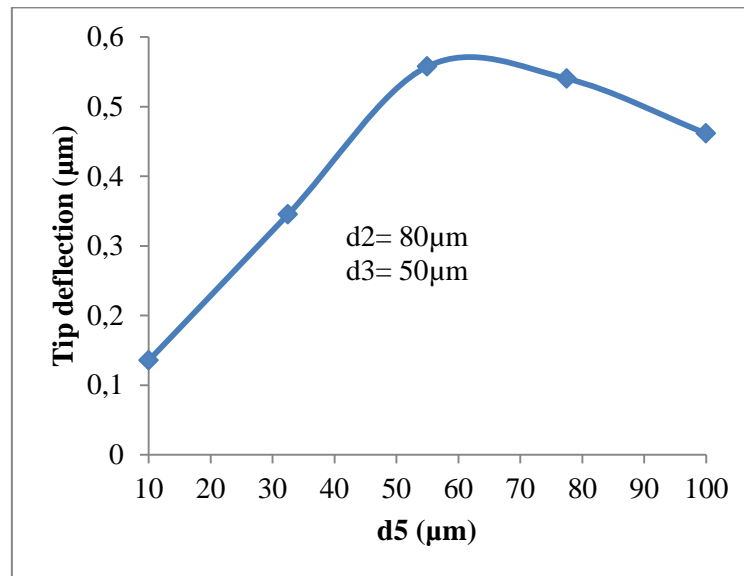


Figure 36: Relation between parameter d_5 and tip deflection of the fin model 1a, when $d_2=80\mu\text{m}$, $d_3=50\mu\text{m}$ and $d_6=50\mu\text{m}$.

The tip deflection increase until $d_5=55\mu\text{m}$, where there is a maximum.

- Maximum tip deflection when $d_6 = 50\mu\text{m}$ is reached with $d_2 = 80\mu\text{m}$, $d_3 = 50\mu\text{m}$ and $d_5 = 55\mu\text{m}$ and its value is **$0.558\mu\text{m}$** .

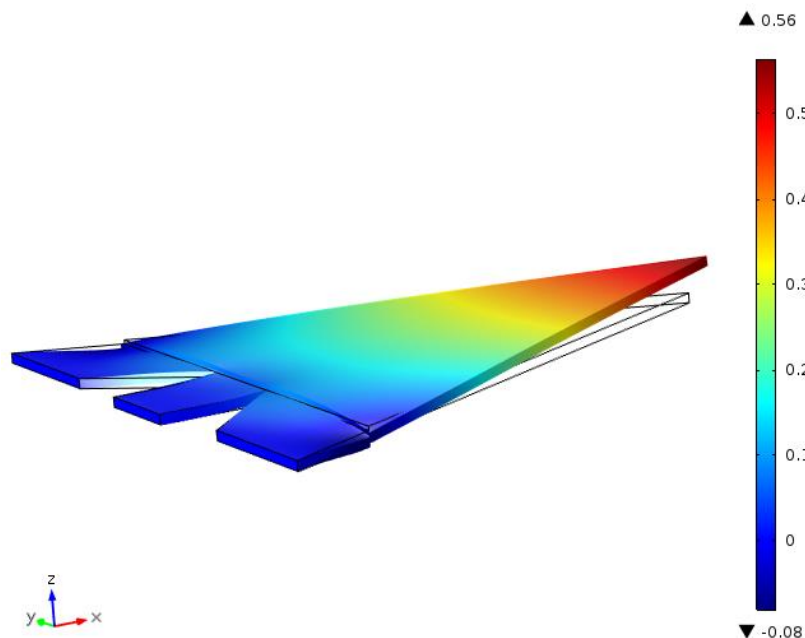


Figure 37: Tip deflection reached in model 1a when $d_6=50\mu\text{m}$ and $\Delta T=60\text{K}$.

- Maximum tip deflection when $d_6 = 100\mu\text{m}$ is reached with $d_2 = 80\mu\text{m}$, $d_3 = 50\mu\text{m}$ and $d_5 = 77.5\mu\text{m}$ and its value is **$0.525\mu\text{m}$** .

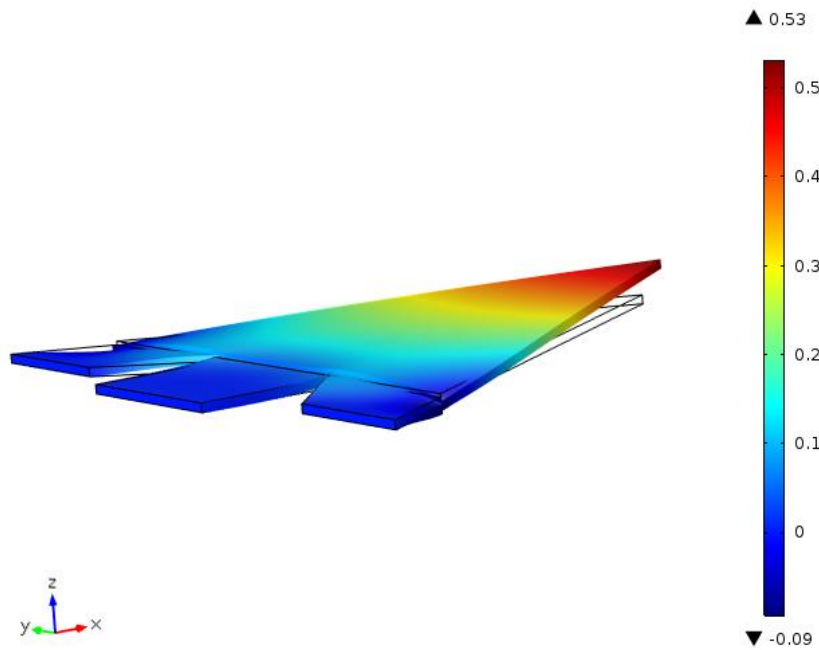


Figure 38: Tip deflection reached in model 1a when $d6=100\mu\text{m}$ and $\Delta T=60\text{K}$.

It is seen that parameter $d6$ do not have a lot of impact on tip deflection, because both results are similar. However, it is preferable model 1a when $d6=50\mu\text{m}$.

b) Model 1b

The same strategy is followed for the design showed in figure 34.

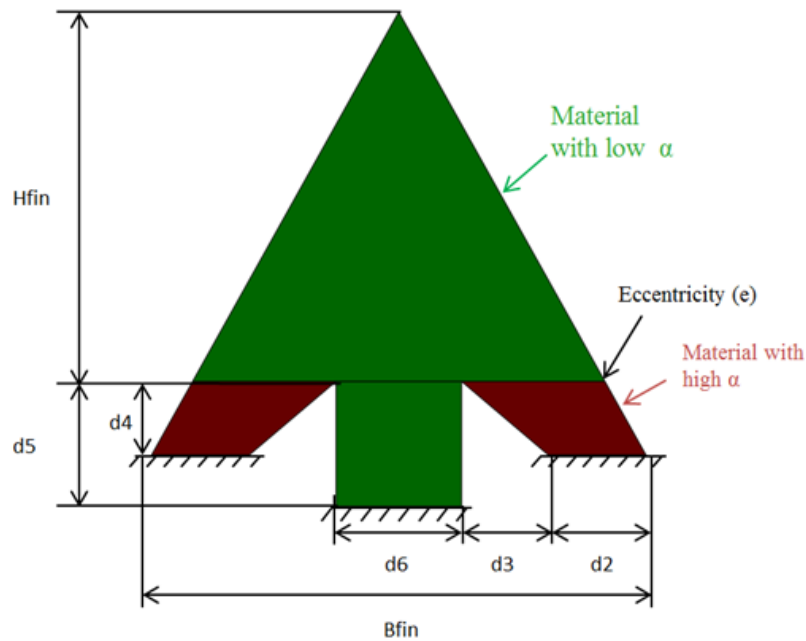


Figure 39: Description and parameters of triangular fin model 1b.

Table 15 shows the constant and variable dimensions of model 1b.

Table 16: Dimensions of triangular fin model 1b.

Constant parameters	
ΔT (K)	60
e (μm)	2
w_{fin} (μm)	5
H_{fin} (μm)	300
T_{ref} (K)	293,15
$d5$ (μm)	20
Variable parameters	
$d2$ (μm)	range [20,32.5,150]
$d3$ (μm)	range [10,10,50]
$d4$ (μm)	range [50,37.4,200]
$d6$ (μm)	50 / 100

The simulation has done 125 combinations. The influence of variable parameters has been evaluated for $d6 = 50\mu\text{m}$ and $d6 = 100\mu\text{m}$, respectively.

- Influence of parameter $d2$:

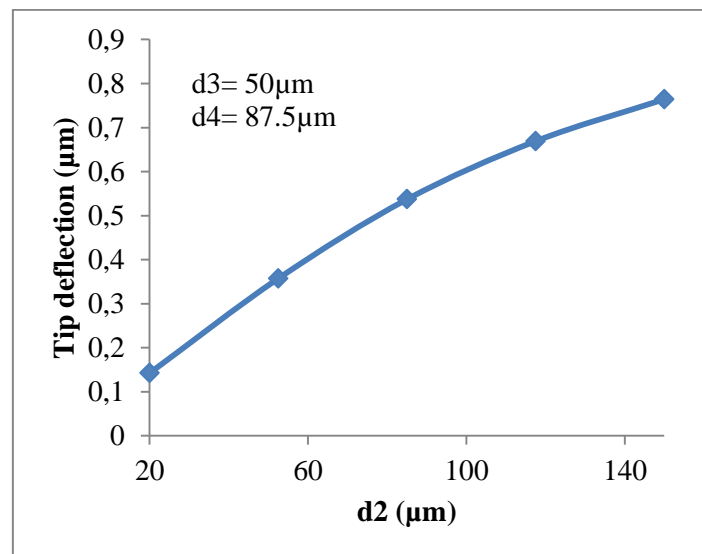


Figure 40: Relation between parameter $d2$ and tip deflection of the fin model 1b, when $d3=50\mu\text{m}$, $d4=87.5\mu\text{m}$ and $d6=50\mu\text{m}$.

Parameter $d2$ influences tip deflection proportionally. As $d2$ increases, tip deflection rises.

- Influence of parameter d3:

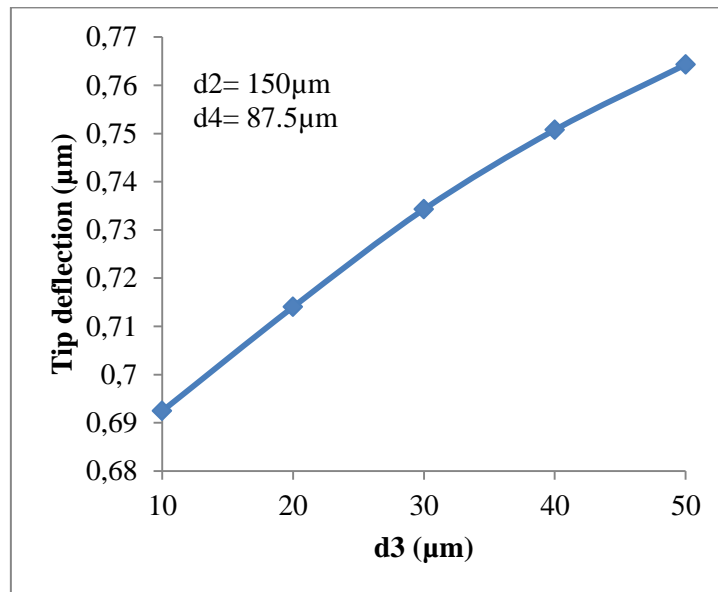


Figure 41: Relation between parameter d3 and tip deflection of the fin model 1b, when d2=150 μm, d4=87,5 μm and d6=50 μm.

Like parameter d2, parameter d3 is proportionally to the tip deflection, but in this case the increase is not as bigger as before.

- Influence of parameter d4:

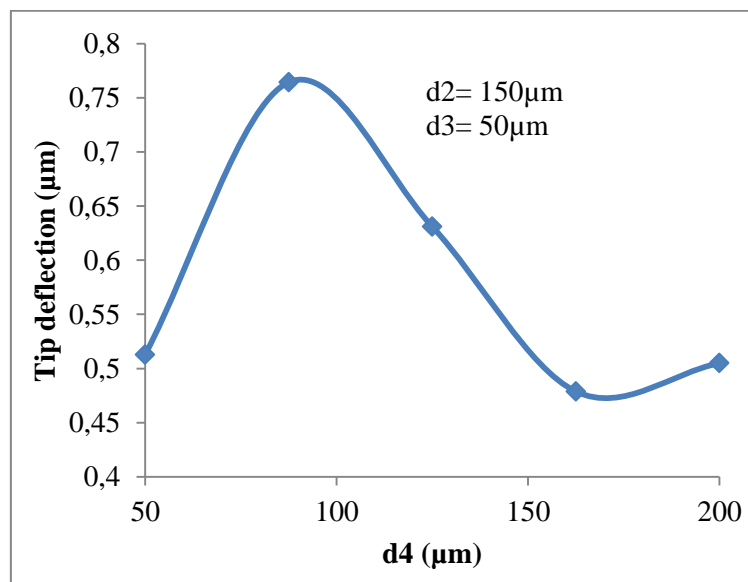


Figure 42: Relation between parameter d4 and tip deflection of the fin model 1b, when d3=50μm, d2=150μm and d6=50μm.

In figure 43 shows the influence of d4 in the tip deflection of the fin. There is a maximum in d4= 87.5μm.

- Maximum tip deflection when $d_6 = 50\mu\text{m}$ is reached with $d_2 = 150\mu\text{m}$, $d_3 = 50\mu\text{m}$ and $d_5 = 87.5\mu\text{m}$ and its value is **$0.764\mu\text{m}$** .

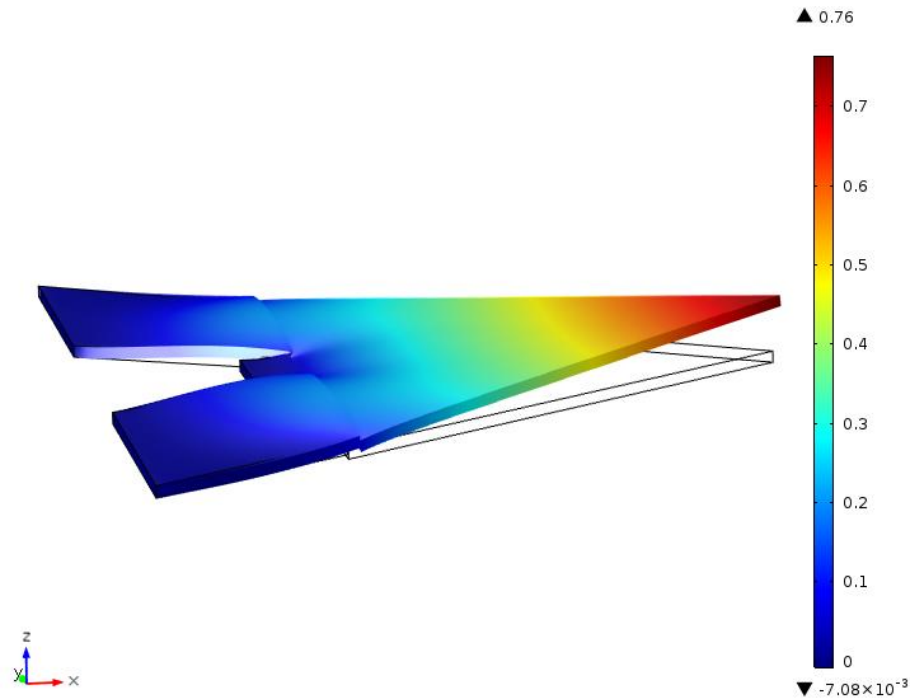


Figure 43: Tip deflection reached in model 1b when $d_6=50\mu\text{m}$ and $\Delta T=60\text{K}$.

- Maximum tip deflection when $d_6 = 100\mu\text{m}$ is reached with $d_2 = 150\mu\text{m}$, $d_3 = 30\mu\text{m}$ and $d_4 = 87.5\mu\text{m}$ and its value is **$0.510\mu\text{m}$** .

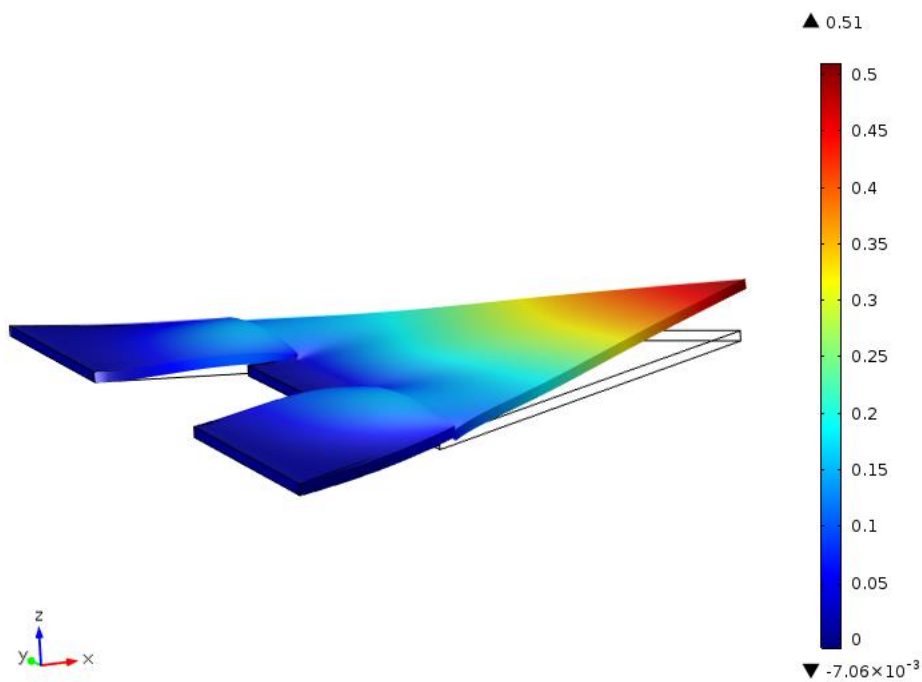


Figure 44: Tip deflection reached in model 1b when $d_6=100\mu\text{m}$ and $\Delta T=60\text{K}$.

About parameter d_6 , when $d_6=50\mu\text{m}$ the tip deflection of the fin is bigger.

5.5.2. Model 2

Following the concept of triangular fins, another design is represented in figure 46. In this case the fin has a fixed point in the centre. There are two strips joined with the fin in one side and fixed at the Si base in the other one. They are fabricated with a material with high CTE, so when they are submitted to high temperatures they have a linear expansion. Thus, a compression force is produced and it is applied at both sides of the fin. Due to embedded point at the centre, the fin rises up.

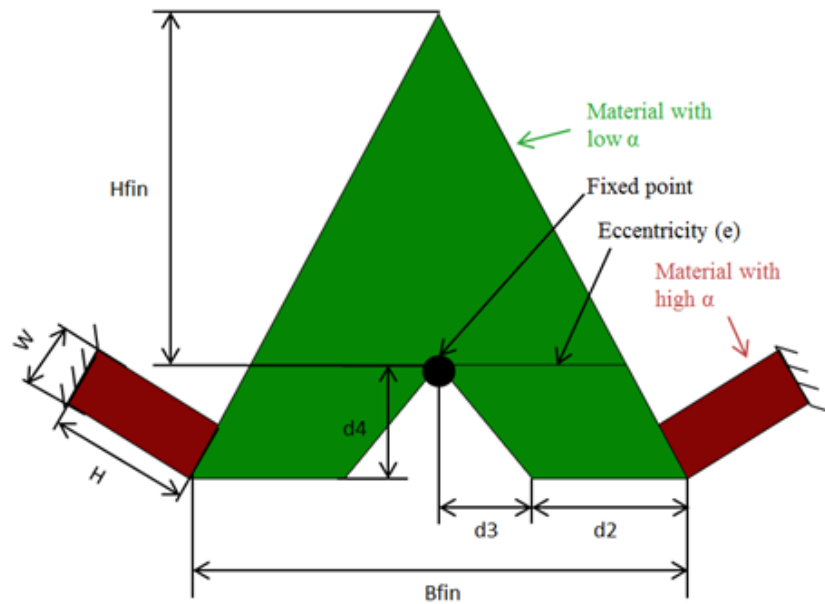


Figure 45: Description and parameters of triangular fin model 2.

Table 16 shows the constant and variable dimensions.

Table 17: Dimensions of triangular fin model 2.

Constant parameters	
ΔT (K)	60
e (μm)	2
w_{fin} (μm)	5
H_{fin} (μm)	300
T_{ref} (K)	293,15
H (μm)	20
L (μm)	50
Variable parameters	
d_2 (μm)	range [10,22.5,100]
d_3 (μm)	range [10,22.5,100]
d_4 (μm)	range [50,37.4,200]

The simulation has done 125 combinations. The influence of variable parameters has been evaluated.

- Influence of d2:

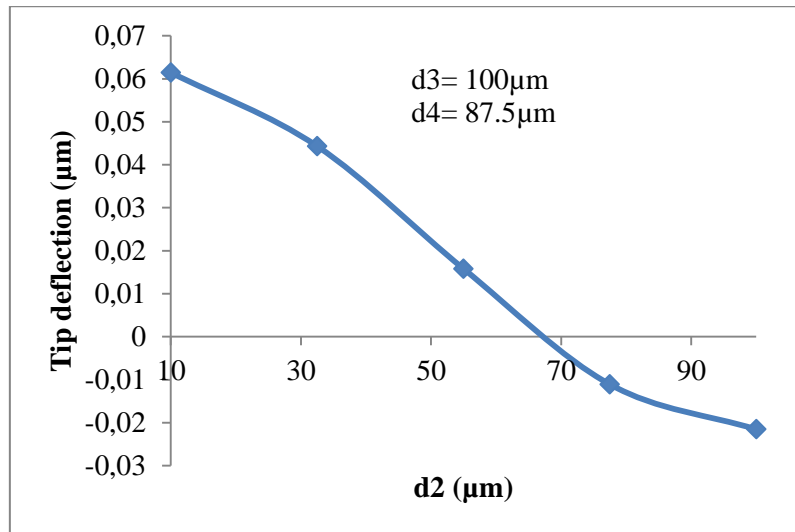


Figure 46: Relation between parameter d2 an tip deflection of model 2, when d3=100μm and d4=87.5μm.

Figure 47 shows that bigger tip deflection is reached when d2 is the smallest.

- Influence of d3:

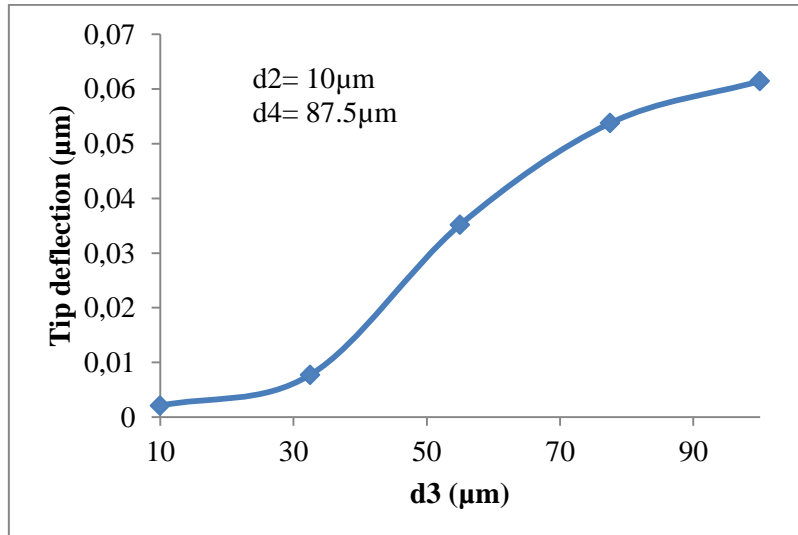


Figure 47: Relation between parameter d3 an tip deflection of model 2, when d2=10μm and d4=87.5μm.

It is seen that tip deflection increases as d3 increases, too.

- Influence of d_4 :

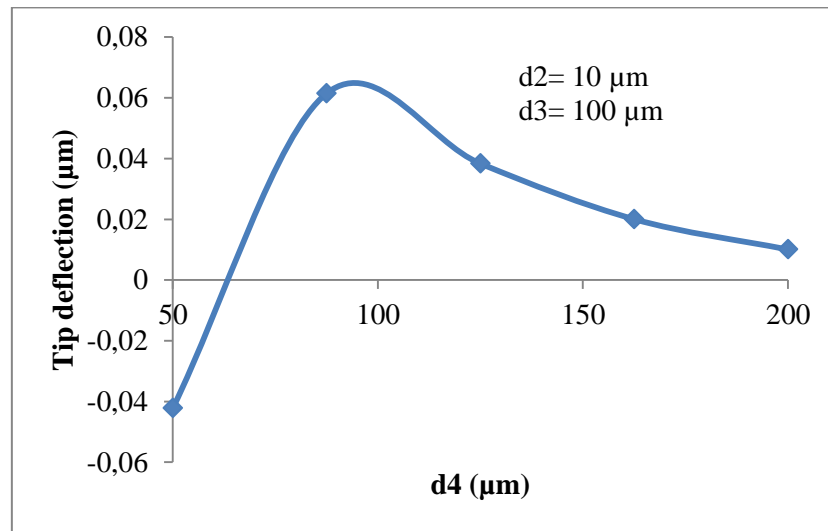


Figure 48: Relation between parameter d_4 and tip deflection of model 2, when $d_2=10\mu\text{m}$ and $d_3=100\mu\text{m}$.

The highest tip deflection is reached for $d_4=87.5\mu\text{m}$, where there is a maximum.

To conclude, d_2 and d_3 have influence on tip deflection. When d_2 is the lowest and d_3 is the highest, the tip deflection of the fin is the greatest.

Therefore, maximum tip deflection is reached with $d_2 = 10\mu\text{m}$, $d_3 = 100\mu\text{m}$ and $d_4 = 87.5\mu\text{m}$ and its value is **0.0614 μm** .

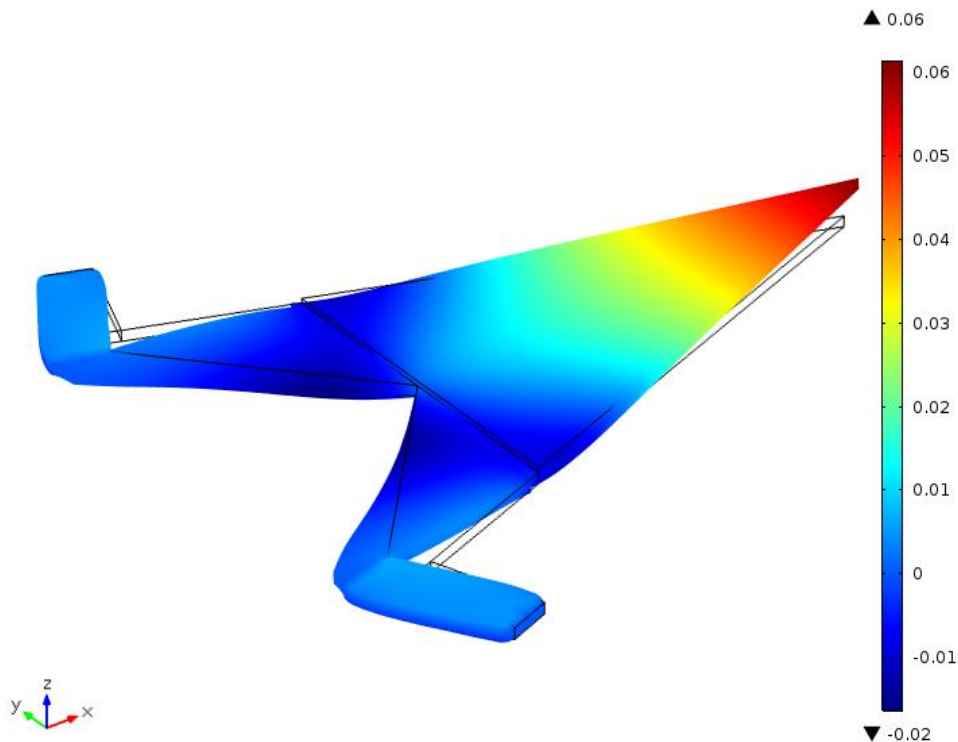


Figure 49: Tip deflection reached in model 2 when $\Delta T=60\text{K}$.

6. Conclusion

After all the results obtained, a comparison between the entire fins model designed and studied is done (Figure 50), but also some conclusions can be established:

- Bimetallic beams have a higher tip deflection than triangular fins in the same conditions and application. The increase is approximately of the 99%.
- The bimetallic beams with an increase of temperature of 60°C have a tip deflection approximately of 50µm. That means they are able to create big LVGs and improve the heat transfer enhancement.
- The triangular fins have a tip deflection lower than 1 µm, so they do not create big LVGs, thus their implementation do not improve the heat transfer enhancement.
- The micro valves are well complemented with the bimetallic strips but on their own, the maximum deflection reached is lower than 1µm. That means that the microvalve cannot do big LVGs itself.
- The mathematical study is easier in bimetallic strips than in triangular fins.
- The combination of materials with different coefficient of expansion is a good solution to fabricate self-adaptive micro fins.

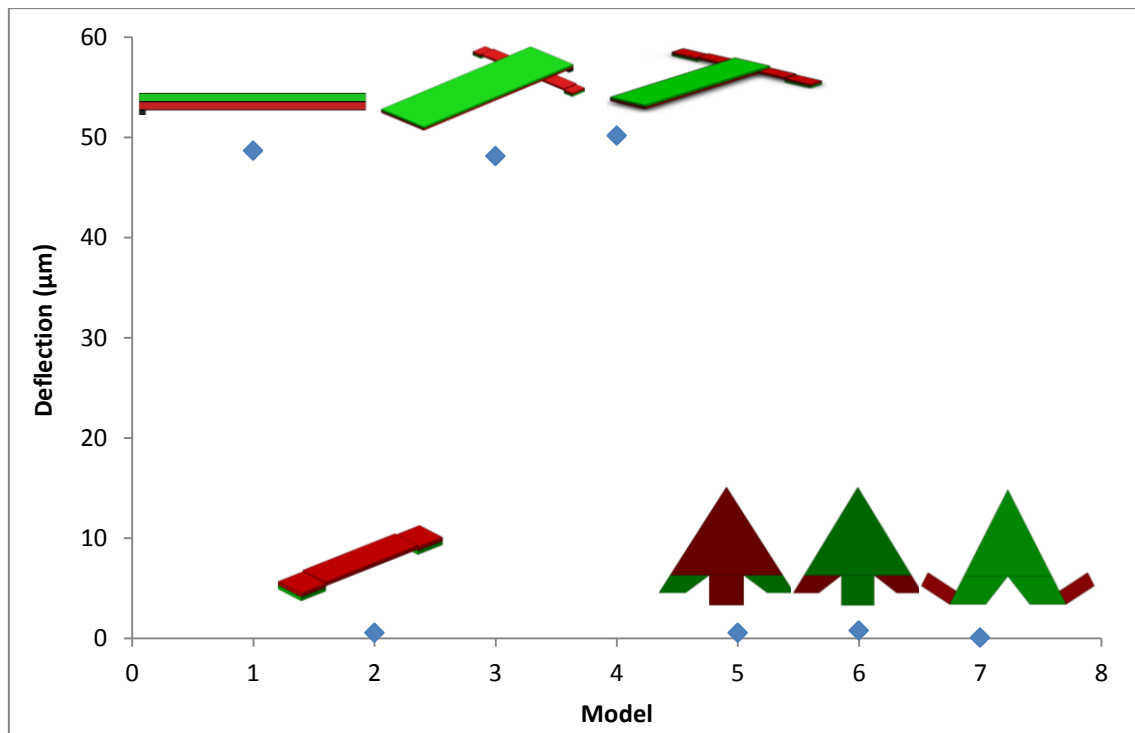


Figure 50: Comparison between all the designs studied.

Bibliography

- [1] A. C. Fischer, «Integrating MEMS and ICs,» *Microsystems & Nanoengineering 1*, pp. 1-16, 2015.
- [2] D. B. Tuckerman, «High-performance heat sinking for VLSI,» *IEEE electron device letters 5*, vol. 2, pp. 126-129, 1981.
- [3] H. Ahmed, «An overview on heat transfer augmentation using vortex generators and nanofluids: Approaches and applications,» *Renewable and sustainable energy reviews 16*, n° %15951-5993, 2012.
- [4] C. Chen, «A study on fluid flow and heat transfer in rectangular microchannels with various longitudinal vortex generators,» *International journal of heat and mass transfer 69*, n° %1203-214, 2014.
- [5] J. Marschewski, «Significant heat transfer enhancement in microchannels with herringbone-inspired microstructures,» *International Journal of Heat and Mass Transfer 95*, pp. 755-764, 2016.
- [6] G. Wang, «Experimental and numerical investigation of a microchannel heat sink (MCHS) with micro-scale ribs and grooves for chip cooling,» *Applied Thermal Engineering 85*, pp. 61-70, 2015.
- [7] S. Riera, «Experimental demonstration of a tailored-width microchannel heat exchanger configuration for uniform wall temperature,» *Journal of Physics: Conference Series 476*, n° %1012075, 2013.
- [8] J. Barrau, «An experimental study of a new hybrid jet impingement/micro-channel,» *Applied Thermal Engineering 30*, pp. 2068-2066, 2010.
- [9] A. Arnaud, «Thermo-mechanical efficiency of the bimetallic strip heat engine at the macro-scale and micro-scale,» *Journal of Micromechanics and Microengineering 25*, pp. 1-13, 2015.
- [10] M. McCarthy, «Thermal buckling of eccentric microfabricated nickel beams as,» *Sensors and Actuators A: Physical 134*, pp. 37-46, 2007.
- [11] C. Doring, «MICROMACHINED THERMOELECTRICALLY DRIVEN CANTILEVER,» *Micro Electro Mechanical Systems 92*, pp. 4-7, 1992.
- [12] W.-H. Chu, «Analysis of tip deflection and force of a bimetallic cantilever microactuator,» *J. Micromech. Microeng. 3*, pp. 4-7, 1993.
- [13] V. Yadav, «Numerical investigation of heat transfer in extended surface microchannels,» *International Journal of Heat and Mass Transfer 93*, pp. 612-622, 2016.
- [14] N. Choudhary, «Shape memory alloy thin films and heterostructures for MEMS applications: A review,» *Sensors and Actuators A: Physical 242*, pp. 162-181, 2016.
- [15] C. A. d. N. Oliveira, «Thermomechanical Analysis on Ti-Ni Shape Memory Helical Springs Under Cyclic Tensile Loads,» *Materials Research 18*, pp. 17-24, 2015.
- [16] M. N. Q., «Influence of Composition and Thermomechanical Training Process on the Transformation Behavior and Shape Memory Properties of NiTi Based Alloys,» *Transactions of the Indian Institute of Metals 66*, pp. 239-275, 2013.
- [17] Y. A. Çengel, *Transferencia de calor y masa: Un enfoque practico*, México DF: MCGRAW-HILL/INTERAMERICANA EDITORES, S.A. DE C.V., Tercera edición 2007.

Appendix

1. Microvalve

1.1. Maximum deformation

Main script

```
%Maximum deformation in function of increase of temperature
clear all

%Data
k1=235; %Thermal conductivity Al [W/mK]
alpha1=23.1e-6; %Coefficient of thermal expansion Al[°C^-1]
E=70*10^10; %Young's Modulus [N/m^2]
k2=148; %Thermal conductivity Si [W/mK]
alpha2=3*10^-6; %Coefficient of thermal expansion Si[°C^-1]
deltalpha=alpha1-alpha2; %Difference of CTE [°C^-1]
L=300*10^-6; %Length of bimetallic strip (without fixed part) [m]
w=50*10^-6; %width [m]
h=[1,2,3,4,5,6]*10^-6; %thickness[m]
e=[0.5,1,2]*10^-6; %Eccentricity [m]

%Iteration variables
n=50;
m=length(h);

%Vectors
deltaT=linspace(40,80,n);
for i=1:3
    for j=1:6
        epsilon(i,j)=e(i)/h(j);
    end
end

%Calculation of maximum deformation for different dimensions and for
different increase of T
for i=1:n
    dA(i)=defmax(e(1),L,h(1),deltaT(i),deltalpha);
    dB(i)=defmax(e(1),L,h(2),deltaT(i),deltalpha);
    dC(i)=defmax(e(1),L,h(3),deltaT(i),deltalpha);
    dD(i)=defmax(e(1),L,h(4),deltaT(i),deltalpha);
    dE(i)=defmax(e(1),L,h(5),deltaT(i),deltalpha);
    dF(i)=defmax(e(1),L,h(6),deltaT(i),deltalpha);
    dG(i)=defmax(e(2),L,h(1),deltaT(i),deltalpha);
    dH(i)=defmax(e(2),L,h(2),deltaT(i),deltalpha);
    dI(i)=defmax(e(2),L,h(3),deltaT(i),deltalpha);
    dJ(i)=defmax(e(2),L,h(4),deltaT(i),deltalpha);
    dK(i)=defmax(e(2),L,h(5),deltaT(i),deltalpha);
    dL(i)=defmax(e(2),L,h(6),deltaT(i),deltalpha);
    dM(i)=defmax(e(3),L,h(1),deltaT(i),deltalpha);
    dN(i)=defmax(e(3),L,h(2),deltaT(i),deltalpha);
    dO(i)=defmax(e(3),L,h(3),deltaT(i),deltalpha);
    dP(i)=defmax(e(3),L,h(4),deltaT(i),deltalpha);
    dQ(i)=defmax(e(3),L,h(5),deltaT(i),deltalpha);
    dR(i)=defmax(e(3),L,h(6),deltaT(i),deltalpha);
end
```

```
%Critical increase of temperature
for i=1:m
    deltaTcr(i)=(pi*h(i))^2/(12*deltalpha*L^2);
end

%Representation of curves
figure(1)
hold on
plot(deltaT,dA,'r',deltaT, dB,'b',deltaT,dC,'c',deltaT,dD,'g',deltaT,dE,
'black',deltaT,dF,'m');
plot(deltaT,dG,'*',deltaT,dH,'*',deltaT,dI,'*',deltaT,dJ,'*',deltaT,dK,
'*',deltaT,dL,'*');
plot(deltaT,dM,'--',deltaT,dN,'--',deltaT,dO,'--',deltaT,dP,'--',
'deltaT,dQ,'--',deltaT,dR,'--');
legend('dA','dB','dC','dD','dE','dF','dG','dH','dI','dJ','dK','dL','dM',
'dN','dO','dP','dQ','dR')
xlabel('Increment de temperatura (deltaT)')
ylabel('Deformació màxima (m)')
grid on
```

Function of maximum deformation

```
%Function of maximum deformation

function f=defmax(e,L,h,deltaT,deltalpha)
f=e*(sec((L*sqrt(deltalpha*deltaT*12))/(2*h))-1);
end
```

1.2. Non-dimensional curves

Main script

```
%Maximum non-dimensional deflection in function of non-dimensional
temperature
clear all

%Data
alpha1=23.1e-6; %Coefficient of thermal expansion Al[°C^-1]
alpha2=3*10^-6; %Coefficient of thermal expansion Si[°C^-1]
deltalpha=alpha1-alpha2; %Difference of CTE [°C^-1]
L=300*10^-6;%Length of bimetallic strip (without fixed part) [m]

%iteration variables
m=6;
n=100;
o=3;

%Vectors
h=linspace(1,6,m)*10^-6; %Width bimetallic strip's layer [m]
e=linspace(0.7,3,o)*10^-6; %Eccentricity [m]
theta=linspace(0,1,n); %Non-dimensional temperature [deltaT/deltaTcr]
deltaT=linspace(40,80,n); %Increase of temperature

%Delta-theta curves for each epsilon
for i=1:o
    for j=1:m
```

```

        epsilon1(i,j)=e(i)/h(j);
    end
end

epsilon2=horzcat(epsilon1(1,:),epsilon1(2,:));
epsilon=sort(epsilon2);
l=length(epsilon);

for i=1:l
    for j=1:n
        ita1(i,j)=secant(epsilon(i),theta(j));
        d(i,j)=epsilon(i)*(sec(ita1(i,j))-1);
    end

    %Delta-theta curves for each epsilon
    hold on
    plot(theta(:),d(i,:))
    xlabel('theta')
    ylabel('delta')

    legend('epsilon=0.1167','epsilon=0.14','epsilon=0.175','epsilon=0.2333',
        'epsilon=0.3083','epsilon=0.35','epsilon=0.37','epsilon=0.4625','eps
        ilon=0.6167','epsilon=0.7','epsilon=0.925','epsilon=1.85')
end

```

Secant method

```

%Secant method to obtain ita
function f=secant(epsilon,theta)
XX=inici(epsilon);
    for i=1:2
        YY(i)=EEf(XX(i),epsilon,theta);
    end
y=1;
n=1;
    while ((abs(y)>1e-15)&&(n<80))
        f=XX(2)-YY(2)*((XX(2)-XX(1))/(YY(2)-YY(1)));
        y=EEf(f,epsilon,theta);
        XX(1)=XX(2);
        YY(1)=YY(2);
        XX(2)=f;
        YY(2)=y;
        n=n+1;
    end
end

```

Error function (related with the secant method)

```

%Error function
function f=EEf(ita,epsilon,theta)
f=(2*ita/pi)^2*(1+(3*epsilon^2/4)*((tan(ita)*cos(4*ita))/(2*ita)+tan(i
ta)^2*(1+sin(4*ita)/(4*ita))+(1-sin(4*ita)/(4*ita))))-theta;
end

```

Initial vectors

```
%Initial vectors for the secant method
function XX=inici(epsilon)
    if epsilon==0
        XX=[0.001,0.0011];
    elseif (0.01<=epsilon)&&(epsilon<=0.04)
        XX=[0.001,0.0011];
    elseif (0.041<=epsilon)&&(epsilon<=0.09)
        XX=[0.003,0.0031];
    elseif (0.091<=epsilon)&&(epsilon<=0.15)
        XX=[1.5,1.6];
    elseif (0.151<=epsilon)&&(epsilon<=0.2)
        XX=[2.1,2.2];
    elseif (0.201<=epsilon)&&(epsilon<=0.3)
        XX=[3.1,3.2];
    elseif (0.301<=epsilon)&&(epsilon<=0.4)
        XX=[4,4.1];
    elseif (0.41<=epsilon)&&(epsilon<=0.5)
        XX=[5,5.1];
    elseif (0.51<=epsilon)&&(epsilon<=0.7)
        XX=[6,6.1];
    elseif (0.71<=epsilon)&&(epsilon<=0.8)
        XX=[7,7.1];
    elseif (0.81<=epsilon)&&(epsilon<=2)
        XX=[1,1.1];
    end
end
```

2. Bimetallic strip

2.1. Impact of width

```
%Impact of width
clear all;

%Variables

dT=60; %(C)
L=300e-06;

% Material 1: SiO2
E1=70e9; %Young's Modulus (Pa)
a1=0.6e-06; %CTE (K^-1)
t1=0.5e-06; %thickness (m)

% Material 2: Al
E2=70e9; %Young's Modulus (Pa)
a2=23e-06; %CTE (K^-1)
t2=0.5e-06; %thickness (m)

n=21; %iteration
b1=linspace(10e-6,100e-6,n);
b2=linspace(10e-6,100e-6,n);

for i=1:n
    I1(i)=(b1(i)*t1^3)/12; %Inertial moment material 1 (kg·m^2)
```

```

A1(i)=b1(i)*t1; %Sectional area material 1 (m^2)

for j=1:n
    I2(j)=(b2(j)*t2^3)/12; %Inertial moment material 2 (kg·m^2)
    A2(j)=b2(j)*t2; %Sectional area material 2 (m^2)
    a=(a2-a1)*dT;

    b(i,j)=(t1+t2/2)+((2/(t1+t2))*(E1*I1(i)+E2*I2(j))*((1/(E1*A1(i)))+(1/(
    E2*A2(j)))));
    k(i,j)=a/b(i,j);
    v(i,j)=k(i,j)*L^2/2;
    j=j+1;
end
i=i+1;
end

[M,I] = max(v(:));
v_max=10e05*M;
[i_max, j_max] = ind2sub(size(v),I);
b1_max=1e06*(90e-06+(10*i_max/1e06));
b2_max=1e06*(70e-06+(10*j_max/1e06));
v*10e05;

figure
mesh(b1,b2,v);
title('Optimal width')
xlabel('b2') % x-axis label
ylabel('b1') % y-axis label
zlabel('d')

```

2.2. Impact of thickness

```

clear all;

%% Variables
dT=60; %(C)
L=300e-06;

% Material 1: SiO2
E1=70e9; %Young's Modulus (Pa)
a1=0.6e-06; %CTE (K^-1)
b1=50e-06; %Width (m)

% Material 2: Al
E2=70e9; %Young's Modulus (Pa)
a2=23e-06; %CTE (K^-1)
b2=50e-06; %Width (m)

n=21; %iteration
for i=1:n
    t1(i)=0.4e-06+(i/1e07); %(from 0.5 to 2.5 microns)
    I1(i)=(b1*t1(i)^3)/12; %Inertial moment material 1 (kg·m^2)

```

```

A1(i)=b1*t1(i); %Sectional area material 2 (m^2)
for j=1:n
    t2(j)=0.4e-06+(j/1e07); %(from 0.5 to 2.5 microns)
    I2(j)=(b2*t2(j)^3)/12; %Inertial moment material 2 (kg·m^2)
    A2(j)=b2*t2(j); %Sectional area material 2 (m^2)
    a=(a2-a1)*dT;

b(i,j)=(t1(i)+t2(j)/2)+((2/(t1(i)+t2(j)))*(E1*I1(i)+E2*I2(j))*((1/(E1*
A1(i)))+(1/(E2*A2(j)))));
    k(i,j)=a/b(i,j);
    v(i,j)=k(i,j)*L^2/2;
    j=j+1;
end
i=i+1;
end

[M,I] = max(v(:));
v_max=10e05*M
[i_max, j_max] = ind2sub(size(v),I);
h1_max=10e05*(0.4e-06+(i_max/1e07))
h2_max=10e05*(0.4e-06+(j_max/1e07))

figure
mesh(t1,t2,v);
xlabel('t_1 (m)') % x-axis label
ylabel('t_2 (m)') % y-axis label
zlabel('d (m)') % z-axis label

```

2.3.Profile of a bimetallic strip submitted to an increase of temperature for differenc heat transfer coefficient

```

%Deformation of bimetallic strip for a determined width, thickness and
heat transfer coefficient
clear all;

% Variables
Tb=70; %Temperature at the base (°C)
Tfluid=25; %Temperature of the fluid (water) (°C)
L=300e-06;

% Material 1: SiO2
E1=70e9; %Young's Modulus(Pa)
a1=0.6e-06; %CTE (K^-1)
b1=100e-06; %width (m)
t1=0.5e-06; %thickness (m)
k1=1.3;

% Material 2: Al
E2=70e9; % Young's Modulus(Pa)
a2=23e-06; %CTE ( K^-1)
b2=100e-06; %Width (m)
t2=0.5e-06; %Thickness (m)
k2=235;

%% Deformation for a determinate h
h1=[2000,10000,50000]; %W/m^2*K

```

```

n=101; %iteration
I1=(b1*t1^3)/12;
A1=b1*t1;
P1=2*b1+2*t1;

I2=(b2*t2^3)/12;
A2=b2*t2;
P2=2*b2+2*t2;
P=P1+P2;

k=(k1*A1+k2*A2)/(A1+A2); % (W/m*K)
A=A1+A2;

%Deformation

for j=1:3
    h(j)=h1(j);
    m(j)=sqrt((h(j)*P)/(k*A)); %m factor
    for i=2:n
        % Temperature distribution
        inc=L/(n-1);
        y(i)=(i-1)*inc; %(from 0 to 150 microns (L))
        T1=(Tb-Tfluid);
        T2(j,i)=cosh(m(j)*(L-y(i)))+(h(j)/(m(j)*k))*sinh(m(j)*(L-y(i)));
        T3(j,i)=(cosh(m(j)*L)+(h(j)/(m(j)*k))*sinh(m(j)*L));
        T(j,1)=Tb;
        T(j,i)=T1*(T2(j,i)/T3(j,i))+Tfluid; %Temperature distribution
        Tc=20; %Temperature of non-curved fin
        dT(j,1)=T(j,1)-Tc;
        dT(j,i)=T(j,i)-Tc;

%First element
        a(j,1)=(a2-a1)*dT(j,1);

b=((t1+t2)/2)+((2/(t1+t2))*(E1*I1+E2*I2)*((1/(E1*A1)))+(1/(E2*A2))));
        kt(j,1)=a(j,1)/b;
        r(j,1)=1/kt(j,1);
        theta(j,1)=(kt(j,1)*inc);
        theta2(j,1)=theta(j,1);
        dy(j,1)=sin(theta(j,1))*inc;
        dy2(j,1)=dy(j,1);

        % Deflection with temperature
        a(j,i)=(a2-a1)*dT(j,i);

b=((t1+t2)/2)+((2/(t1+t2))*(E1*I1+E2*I2)*((1/(E1*A1)))+(1/(E2*A2))));
        kt(j,i)=a(j,i)/b; %curvature

        if kt(j,i)==0
            r(j,i)=0;
        else
            r(j,i)=1/kt(j,i); %radius of curvature
        end
        theta(j,i)=(kt(j,i)*inc); %angle
        theta2(j,i)=theta(j,i)+theta2(j,i-1); %sum of angle
        dy(j,i)=inc*sin(theta2(j,i));
    end
end

```

```
dy2(j,i)=dy(j,i)+dy2(j,i-1);

deflection
    i=i+1;
end
end

%Deflection dy
figure(2)
plot(y,dy2)

xlabel('position along the strip (m)');
ylabel('d (m)');
legend('h=2000 W/m^2K','h=10000 W/m^2K','h=50000 W/m^2K');
grid on
```